



## Syntheses, Crystal Structures, and Single Small Molecule Encapsulation Properties of Cavitand-Porphyrins

Jun Nakazawa, Maki Mizuki, Jun Hagiwara, Yuichi Shimazaki, Fumito Tani, and Yoshinori Naruta\*

Institute for Materials Chemistry and Engineering, Kyushu University, Higashi-ku, Fukuoka 812-8581

Received April 12, 2006; E-mail: naruta@ms.ifoc.kyushu-u.ac.jp

New capsule-shaped hosts “cavitand-linked porphyrin” metal complexes (**Mcp**: M = H<sub>2</sub>, Ni, Zn, and Pd) have been synthesized to mimic the substrate binding functions of metalloenzymes such as cytochrome P-450<sub>cam</sub>. Crystal structures of cavitand **1**·MeOH·CHCl<sub>3</sub>, [Zn**tp**(MeOH)], [Ni**cp**]·MeOH·2CHCl<sub>3</sub>·3H<sub>2</sub>O, [Zn**cp**(MeOH)]·2CHCl<sub>3</sub>·3H<sub>2</sub>O, and [Pd**cp**]·MeOH·2CHCl<sub>3</sub>·3H<sub>2</sub>O have been determined. One methanol molecule, originating from crystallization solvent is encapsulated in each host cavity, and coordinates to Zn in **Zncp** but not in Ni- and **Pdcp**. Encapsulation of various small hydrocarbon molecules in CDCl<sub>3</sub> solutions of **Mcps** have been evaluated by determining binding constants and thermodynamic parameters obtained from <sup>1</sup>H NMR titrations. All **Mcps** encapsulate hydrocarbons smaller than propane under atmospheric pressure. The guest size selectivity is primarily influenced by cavity size, and partly by metal insertion. The metal ion radius does not affect guest size selectivity. Encapsulation of coordinating guest molecules (MeOH, EtOH, MeCN, and H<sub>2</sub>O) in **Mcps** has also been investigated. Only **Zncp** favors coordination of non-hydrocarbon guests such as MeOH. We concluded that accommodation of different size guests by **Mcps** depends upon guest sizes and coordination of functional groups depends upon both the identity of the porphyrin's metal ion and guest sizes.

In biological systems, many enzymes carry out specific reactions (e.g. chiral-, position-, and size-selective reactions), which begin with binding and recognition of substrates in three-dimensional active sites. For example, mono-oxygenation reactions are catalyzed by enzymes such as cytochrome P-450 and methane monooxygenase.<sup>1–3</sup> These enzymes have hydrophobic cavities to bind small hydrocarbon substrates at their active sites, where selective and site-specific oxidation reactions occur. These reactions are notoriously difficult to achieve using artificial catalysts. The process of substrate binding is an important step to consider in design of functional model systems, which mimic enzymatic catalysis. Recently, development of industrial syntheses based on efficient environmentally friendly “green chemistry” reactions catalyzed by enzymes and high-performance enzyme mimicking artificial systems have been attracted a great deal of attention. In this paper, we aim to incorporate appropriate substrate binding functions into potentially artificial catalysts for oxidation of small hydrocarbons such as methane.

In the field of molecular recognition chemistry, many examples of functional group selective recognition using various interaction strategies have been reported.<sup>4</sup> On the other hand, development of host model systems capable of molecular recognition of hydrocarbon molecules has proven to be quite difficult.<sup>5–10</sup> Over the past two decades, most successful examples of the hydrocarbon recognition employed capsule-shaped hosts for selective encapsulations.<sup>11–23</sup> Reversible recognition of small hydrocarbons, such as methane, have not been achieved. Furthermore, many researchers are now examining chemical reactions of encapsulated guests by adding reaction sites to the host systems.<sup>24–26</sup>

We have reported size selective encapsulation of small hydrocarbon molecules into a cavitand-linked free-base porphy-

rin (**H<sub>2</sub>cp**, shown in Chart 1) in a previous communication.<sup>27</sup> We found that **H<sub>2</sub>cp** could encapsulate guests smaller than propane, and that an encapsulated guest molecule could be easily exchanged with a bulk guest molecule in the solution. In addition, the porphyrin can function not only as a capsule bottom of **H<sub>2</sub>cp** but also as a potentially versatile metal active site catalyst.

In this article, we report the syntheses of “cavitand-linked porphyrin” metal complexes (**Mcp**: M = H<sub>2</sub>, Ni, Zn, and Pd) and disclose crystal structures for **Nicp**, **Zncp**, and **Pdcp** as a next step in development and investigation of encapsulation properties of artificial systems having recognition functions similar to those of metalloenzymes. Since the method of choice for investigation of encapsulation behavior of small hydrocarbons is NMR, we chose Zn<sup>II</sup>, Ni<sup>II</sup>, and Pd<sup>II</sup> for this study. Encapsulation properties of **Mcps** for various small hydrocarbon molecules arise from difference of the metal ions in the porphyrin as indicated by titrations monitored by <sup>1</sup>H NMR. The guest size selectivity caused by metal insertion and metal ion radius difference is investigated by comparisons of the effects of these properties on the encapsulation process. In addition, we report the results of encapsulations of coordinating guest molecules (methanol, ethanol, acetonitrile, and water) to the metal ions by comparisons among **H<sub>2</sub>cp**, **Zncp**, **Nicp**, and **Pdcp**.

### Results and Discussion

**Host Design.** A host molecule which can encapsulate and retain a single small hydrocarbon molecule within its cavity for a significant period of time should fulfill following conflicting requirements: (1) Since one does not expect to stabilize guest-encapsulation by strong interactions between a host molecule and a hydrocarbon, only the steric blockage of a

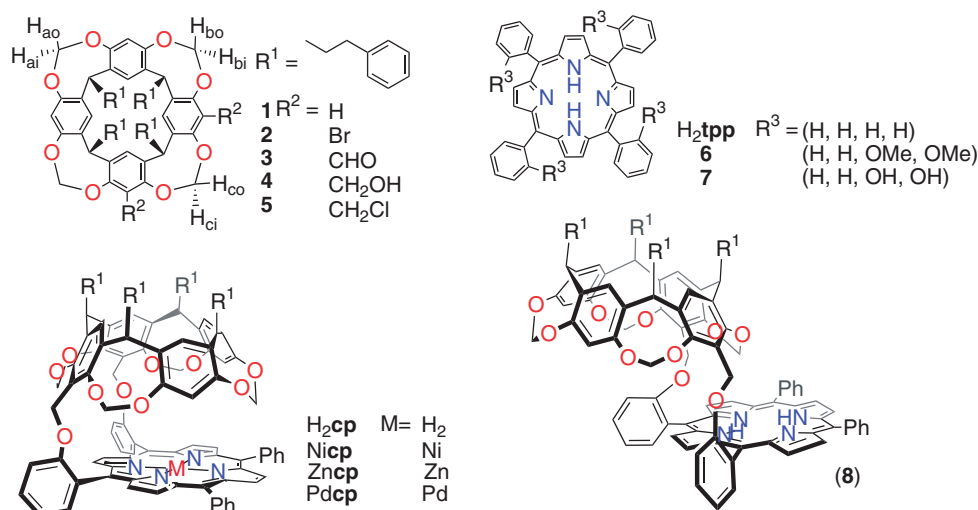
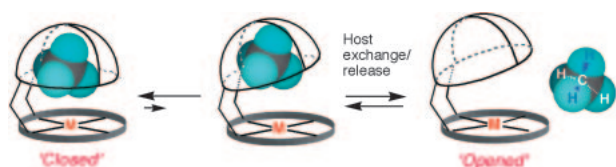


Chart 1.



Scheme 1.

hydrocarbon guest by host cavity will prevent the guest from escaping from the cavity. Thus, the portal of the host should be small enough to prevent quick release of a guest while still enabling exchange of the guest with molecules of the bulk solvent phase. (2) If the portal is too small, the guest molecule will either not enter the cavity or else not be released following encapsulation. (3) During the synthesis of a host or during its molecular recognition/reaction with substrates, inclusion of a solvent molecule within the cavity should be absolutely avoided.

In order to satisfy these requirements, the host molecule should have a small cavity, suitable only for encapsulation of a small hydrocarbon molecule. For the guest exchange to occur at a moderate rate, the host molecule's portal should be open only to an optimal timescale (Scheme 1). To meet these criteria, a cavitand-linked porphyrin (**cp**) was designed to allow sufficient portal size of its "open" form with appropriate molecular dynamics. The cavitand is linked by two ether linkages at the 5,10-phenyl groups to retain flexibility in cooperation with deformation of the porphyrin ring.

**Synthesis of M<sub>cp</sub>.** The compounds discussed herein and the synthetic intermediates of M<sub>cp</sub>s are shown in Chart 1. The starting material of the cavitand moiety of M<sub>cp</sub>, dibromocavitand (**2**) was prepared as previously published.<sup>28–30</sup> Diformylcavitand (**3**) was obtained by lithiation and subsequent formylation of **2**. In this step, monoformylcavitand was unavoidably formed as a by-product. The mixture of **3** and monoformylcavitand could be separated by silica-gel column chromatography. **3** was reduced to bis(hydroxymethyl)cavitand (**4**) by lithium tetrahydridoaluminate in a quantitative yield. The chlorination of **4** was carried out with *N*-chlorosuccinimide and dimethyl sulfide to give bis(chloromethyl)cavitand (**5**).<sup>31–33</sup>

For the porphyrin moiety, *meso*-bis(methoxyphenyl)diphenylporphyrin (**6**) was synthesized by the Adler method from pyrrole, benzaldehyde, and *o*-anisaldehyde.<sup>34</sup> This reaction afforded a mixture of six differently substituted porphyrins including *meso*-tetraphenylporphyrin ( $H_2tpp$ ). Because separation of  $\alpha\alpha$ -,  $\alpha\beta$ -, 5,10-, and 5,15-disubstituted isomers in **6** was difficult, we carried out demethylation of mixture **6**, and obtained a *meso*-bis(hydroxyphenyl)diphenylporphyrin mixture (**7**),<sup>35</sup> which contains four isomers ( $\alpha\alpha$ - and  $\alpha\beta$ -atropisomers of 5,10- and 5,15-isomers (2:1)). The atropisomer immediately interconverted between  $\alpha\alpha$  and  $\alpha\beta$  even at room temperature, and separation by silica-gel column chromatography was not possible. Thus, **7** was employed without separation in the subsequent condensation reaction.

$H_2cp$  was synthesized by Williamson ether synthesis from bis(chloromethyl)cavitand (**5**) with a bis(*o*-hydroxyphenyl)porphyrin stereoisomeric mixture **7** in *N*-methylpyrrolidone and THF under basic conditions.<sup>27,33</sup> Interestingly, the desirable *syn*-isomer  $H_2cp$  (46% yield based on **5**) was preferentially obtained as a main product over the *anti*-isomer **8** (14% yield) even with use of a mixture of four atropisomers and regioisomers. Both were separated by silica-gel column chromatography. In general, it is considered that the reaction of *meso*-disubstituted porphyrin stereoisomeric mixture **7** with **5** mixed at nearly a 1:1 molar ratio produces many products. However, the reaction produced 60% total yield of  $H_2cp$  and **8** based on **5**.<sup>36</sup> In other words,  $H_2cp$  and **8** were obtained almost quantitatively from the 5,10-substituted porphyrin isomer (theoretical yield  $\approx 66\%$ ). The configurations of the *syn*-( $H_2cp$ ) and *anti*-(**8**) isomers were confirmed by <sup>1</sup>H NMR spectroscopy and crystal structures of M<sub>cp</sub>s (described in the next section).<sup>27</sup> In the <sup>1</sup>H NMR spectra of  $H_2cp$ , signals of  $H_{ai}$  (at  $-1.13$  ppm) and  $H_{bi}$  (at 2.21 ppm) in the cavitand moiety (Fig. 1) are shifted upfield relative to those of bis(chloromethyl)cavitand **5** (at 4.73 and 4.63 ppm, respectively) (shown in Chart 1) due to the large anisotropic effect of the porphyrin ring current. In contrast, signals of  $H_{ai}$  and  $H_{bi}$  of the *anti*-isomer **8** are shifted down-field relative to those of **5**. This observation suggests that the cavitand and porphyrin moieties of  $H_2cp$  adopt a fully overlapping geometry and the cavity portal is very narrow.

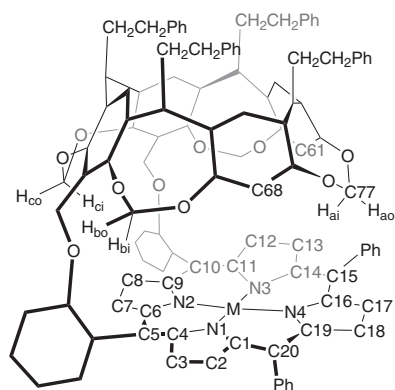


Fig. 1. Labeling of selected atoms of **Mcps**.

As indicated by NMR, none of the solvents were incorporated in the cavity.

**Nicp**, **Zncp**, and **Pdcp** were synthesized from **H<sub>2</sub>cp** with  $\text{Ni}(\text{AcO})_2$ ,  $\text{Zn}(\text{AcO})_2$ , and  $\text{PdCl}_2$ , respectively and then purified by alumina-column chromatography. Metal insertion into **cp** required more severe conditions than were required for the corresponding tetraphenylporphyrin. This requirement could be caused by steric hindrance around the porphyrin of **H<sub>2</sub>cp** or by poor flexibility of the porphyrin caused by the connected cavitant.<sup>37,38</sup>

Cavitant (**1**) and *meso*-tetraphenylporphyrinzinc(II) complex (**Zntpp**) were synthesized according to literature procedures.<sup>37,39</sup>

Crystal structure of **Mcp**, **Zntpp**, **1**, and **Mcps** ( $M = \text{Zn}, \text{Ni}$ , and  $\text{Pd}$ ) were recrystallized by the diffusion of the chloroform solution to methanol. Crystals were obtained of [**Zntpp**·(MeOH)] (red prism), **1**·CHCl<sub>3</sub>·MeOH (colorless prism), [**Nicp**]·MeOH·2CHCl<sub>3</sub>·3H<sub>2</sub>O (brown platelet), [**Zncp**(MeOH)]·2CHCl<sub>3</sub>·3H<sub>2</sub>O (red platelet), and [**Pdcp**]·MeOH·2CHCl<sub>3</sub>·3H<sub>2</sub>O (orange platelet). With the exception of **Zntpp**, all crystals were efflorescent out of their mother liquid. The formula of the compounds obtained from elemental analyses with vacuum drying were partially depleted in solvent molecules relative to solvent molecules observed in the crystal structures.

The crystal structures of **Zntpp**, **1**, and **Mcps** ( $M = \text{Zn}, \text{Ni}$ , and  $\text{Pd}$ ) are shown in Fig. 2. Crystallographic data and selected atom distances are summarized in Tables 1 and 2, respectively. In the crystal structure of **Zncp**, two chloroform molecules and three water molecules contribute to the structure but are not contained within the cavity. For **Zncp**, the configuration of the cavitant between the porphyrin is the desired *cis*-form and a hemispherical cavity with a small portal exists above the porphyrin. The Zn atom is coordinated by four porphyrin nitrogen donor ligands of the porphyrin and an oxygen atom of the methanol ligand at the apical position in a distorted square pyramidal geometry, where Zn–O(MeOH) length is 2.253(3) Å. This coordination geometry is similar to those observed in the crystal structures of [**Zntpp**(MeOH)] and [**Zntpp**(H<sub>2</sub>O)], where the Zn–O lengths are 2.216(2) and 2.141 Å, respectively.<sup>40</sup> In **Zncp**, the coordinating methanol is found within the cavity. The distance range between the carbon atom of the methanol and four benzene planes which constitute the cavitant hemisphere is 3.843–4.078 Å which is too far for strong CH/π interactions to occur with a specific benzene

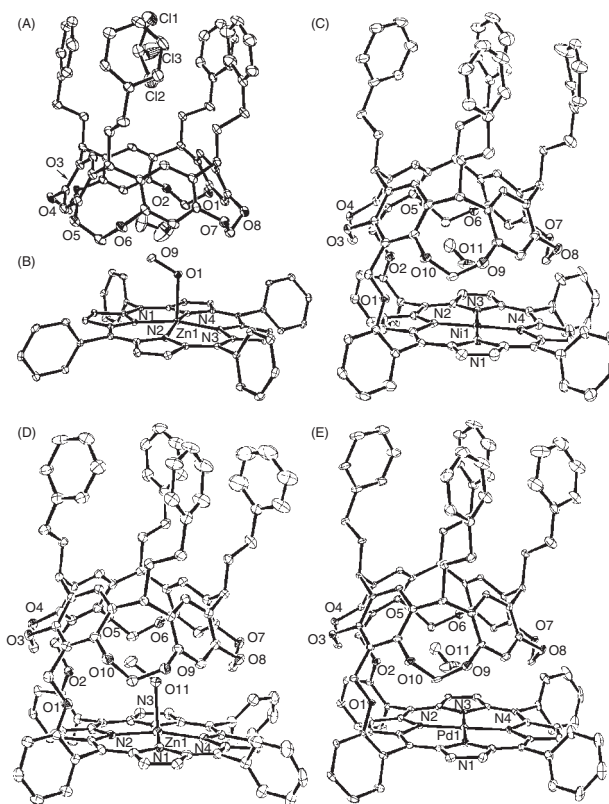


Fig. 2. ORTEP diagrams of (A) **1**·CHCl<sub>3</sub>·MeOH, (B) [**Zntpp**(MeOH)], (C) **Nicp**·MeOH·2CHCl<sub>3</sub>·3H<sub>2</sub>O, (D) [**Zncp**(MeOH)]·2CHCl<sub>3</sub>·3H<sub>2</sub>O, and (E) **Pdcp**·MeOH·2CHCl<sub>3</sub>·3H<sub>2</sub>O with the thermal ellipsoids of 30% probability level. Hydrogen atoms and solvent molecules outside of the cavity in the crystals except **1** are omitted for clarity.

ring.<sup>41</sup> The attractive force between the methyl group of the methanol and the concave surface of the cavitant must be due to van der Waals forces and weak CH/π interactions. One chloroform molecule per cavitant is packed within a groove composed of four CH<sub>2</sub>CH<sub>2</sub>Ph groups. There is a CH/π interaction between the hydrogen of the chloroform and one of the phenyl groups of the groove, where the distance between the carbon atom of chloroform and the proximal phenyl plane is 3.327 Å and the C–H bond of the chloroform is essentially perpendicular to the phenyl plane (see Supporting Information).

In the crystal structure of cavitant **1**, methanol and chloroform molecules form similar adducts. The distance range between the carbon atom of encapsulated methanol and the benzene planes is 3.831–4.099 Å, a range comparable to that observed in the structure of **Zncp**. The distance between the carbon atom of chloroform and a proximal phenyl plane is 3.401 Å and the C–H bond of the chloroform is essentially perpendicular to the phenyl plane as observed form **Zncp**.

Furthermore, both **Nicp** and **Pdcp** crystals also have one methanol molecule in the cavities (C(MeOH)–cavitant benzene planes; **Nicp**: 3.679–3.847, **Pdcp**: 3.681–3.840 Å), and have a CHCl<sub>3</sub> molecule packed in a groove composed of four CH<sub>2</sub>CH<sub>2</sub>Ph moieties as **1** and **Zncp** (C(CHCl<sub>3</sub>)–phenyl plane);

Table 1. Crystallographic Data of **1**, **Zntpp**, **Zncp**, **Nicp**, and **Pdcp**

	<b>1</b> ·MeOH ·CHCl <sub>3</sub>	[ <b>Zntpp</b> (MeOH)]	[ <b>Zncp</b> (MeOH)] ·2CHCl <sub>3</sub> ·3H <sub>2</sub> O	[ <b>Nicp</b> ]·MeOH ·2CHCl <sub>3</sub> ·3H <sub>2</sub> O	[ <b>Pdcp</b> ]·MeOH ·2CHCl <sub>3</sub> ·3H <sub>2</sub> O
Formula	C <sub>66</sub> H <sub>61</sub> Cl <sub>3</sub> O <sub>9</sub>	C <sub>45</sub> H <sub>31</sub> N <sub>4</sub> OZn	C <sub>113</sub> H <sub>96</sub> Cl <sub>6</sub> N <sub>4</sub> O <sub>14</sub> Zn	C <sub>113</sub> H <sub>96</sub> Cl <sub>6</sub> N <sub>4</sub> O <sub>14</sub> Ni	C <sub>113</sub> H <sub>96</sub> Cl <sub>6</sub> N <sub>4</sub> O <sub>14</sub> Pd
Formula weight	1104.56	709.15	2012.12	2005.44	2053.14
<i>T</i> /K	123	123	123	123	123
Crystal size/mm <sup>3</sup>	0.13 × 0.15 × 0.50	0.10 × 0.14 × 0.25	0.30 × 0.20 × 0.10	0.30 × 0.15 × 0.05	0.40 × 0.20 × 0.10
Crystal system	Monoclinic	Triclinic	Monoclinic	Monoclinic	Monoclinic
<i>a</i> /Å	15.928(8)	9.595(2)	12.674(2)	12.635(2)	12.660(5)
<i>b</i> /Å	34.97(2)	11.039(2)	23.706(2)	23.621(2)	23.687(6)
<i>c</i> /Å	15.584(8)	17.888(3)	16.436(1)	16.465(2)	16.491(6)
$\alpha$ /deg	—	99.561(7)	—	—	—
$\beta$ /deg	40.12(3)	104.945(8)	94.263(5)	93.399(5)	93.78(3)
$\gamma$ /deg	—	99.812(7)	—	—	—
<i>V</i> /Å <sup>3</sup>	5592(4)	1759.3(6)	4924.4(9)	4905.5(9)	4934(2)
Space group	<i>P</i> 2 <sub>1</sub> / <i>a</i> (#14)	<i>P</i> 1̄ (#2)	<i>P</i> 2 <sub>1</sub> (#4)	<i>P</i> 2 <sub>1</sub> (#4)	<i>P</i> 2 <sub>1</sub> (#4)
<i>Z</i>	4	2	2	2	2
<i>D</i> <sub>calcd</sub> /g cm <sup>-3</sup>	1.312	1.339	1.357	1.358	1.382
<i>F</i> (000)	2320.00	734.00	2092.00	2088.00	2124.00
$\mu$ (Mo K $\alpha$ )/cm <sup>-1</sup>	2.23	7.40	4.80	4.29	4.18
2 $\theta$ <sub>max</sub> /deg	54.7	55.0	54.9	54.9	55.0
No. of obs reflns	86928	16060	164334	162988	88048
No. of indep reflns	12711	8029	22269	21839	21516
No. of variables	763	588	1338	1377	1348
<i>R</i> <sub>1</sub> [ <i>I</i> > 2 $\sigma$ ( <i>I</i> )] <sup>a)</sup>	0.109	0.055	0.074	0.084	0.077
<i>R</i> <sub>w</sub> (all data) <sup>b)</sup>	0.205	0.148	0.179	0.249	0.191
GOF index	1.207	0.979	1.246	1.041	1.260

a)  $R_1 = \sum ||F_o| - |F_c|| / \sum |F_o|$  for  $I > 2\sigma(I)$  data. b)  $R_w = \{\sum w(|F_o| - |F_c|)^2 / \sum w F_o^2\}^{1/2}$ .

Table 2. Selected Atom Distances (Å) in the Crystals of **1**·MeOH·CHCl<sub>3</sub>, [**Zntpp**(H<sub>2</sub>O)],<sup>40</sup> [**Zntpp**(MeOH)], [**Zncp**(MeOH)]·2CHCl<sub>3</sub>·3H<sub>2</sub>O, [**Nitpp**],<sup>43</sup> [**Nicp**]·MeOH·2CHCl<sub>3</sub>·3H<sub>2</sub>O, [**Pdtpp**],<sup>44</sup> and [**Pdcp**]·MeOH·2CHCl<sub>3</sub>·3H<sub>2</sub>O

	[ <b>Zntpp</b> (H <sub>2</sub> O)]	[ <b>Zntpp</b> (MeOH)]	[ <b>Zncp</b> (MeOH)] ·2CHCl <sub>3</sub> ·3H <sub>2</sub> O	[ <b>Nitpp</b> ]	[ <b>Nicp</b> ]·MeOH ·2CHCl <sub>3</sub> ·3H <sub>2</sub> O	[ <b>Pdtpp</b> ]	[ <b>Pdcp</b> ]·MeOH ·2CHCl <sub>3</sub> ·3H <sub>2</sub> O
Metal–N1(Porphyrin)	2.051	2.068(2)	2.063(4)	1.929	1.952(4)	2.010	2.036(5)
Metal–N2(Porphyrin)	2.039	2.061(2)	2.046(4)	— <sup>a)</sup>	1.958(4)	— <sup>a)</sup>	2.024(4)
Metal–N3(Porphyrin)	2.061	2.058(2)	2.064(4)	— <sup>a)</sup>	1.956(4)	— <sup>a)</sup>	2.027(5)
Metal–N4(Porphyrin)	2.053	2.052(2)	2.052(4)	— <sup>a)</sup>	1.945(4)	— <sup>a)</sup>	2.015(4)
Metal–O(MeOH)	2.141	2.216(2)	2.253(3)	— <sup>b)</sup>	3.27(1)	— <sup>b)</sup>	3.37(2)
C(MeOH)–cavity benzene planes	(to H <sub>2</sub> O) ( <b>1</b> ·MeOH·CHCl <sub>3</sub> ) 3.890, 3.707, 3.831, 4.099		4.038, 3.843, 4.078, 3.916		3.727, 3.815, 3.679, 3.847		3.686, 3.840, 3.681, 3.784
N4–C77	—	—	3.383(7)	—	3.406(6)	—	3.396(7)
C1–C68	—	—	3.880(7)	—	4.117(7)	—	4.195(8)
C14–C61	—	—	4.198(7)	—	3.867(7)	—	3.877(7)
$\Delta M$ <sup>c)</sup>	0.274	0.213	0.213	0.000	–0.008	0.000	–0.011

a) Generated by symmetry operation. b) No axial ligand. c) Displacement of the metal from the least-square plane based on four nitrogen atoms. Positive values are directed to the cavitand moiety and bound methanol.

**Nicp**: 3.349, **Pdcp**: 3.331 Å). The distances between C(MeOH) and the cavitand benzene planes in **1** and **Mcp**s decreases in the following order; **1**  $\approx$  **Zncp** > **Nicp**  $\approx$  **Pdcp**. In the non-coordinating **Mcp**s (M = Ni and Pd), steric repulsion between

the porphyrin of **Mcp** and the MeOH molecule is a dominant interaction and induces MeOH to enter the **Mcp** cavities more deeply than it would enter **1** itself. For **Zncp**, coordination of MeOH to the Zn ion forces the methanol molecule into close

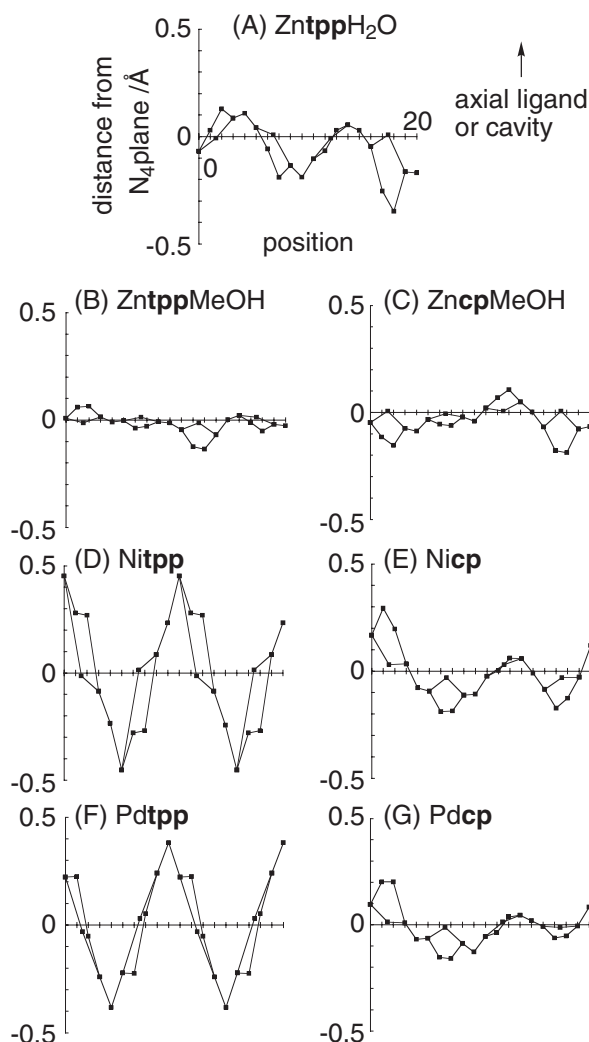


Fig. 3. Distortions of the porphyrin atoms from the least-square plane based on four nitrogen atoms. (A) [Zntpp(H<sub>2</sub>O)],<sup>40</sup> (B) [Zntpp(MeOH)], (C) [Zncp(MeOH)], (D) [Nitpp],<sup>43</sup> (E) [Nicip], (F) [Pdtp],<sup>44</sup> and (G) [Pdcp]. Atom numbering is shown in Fig. 1.

proximity with the porphyrin plane.

To evaluate the cavity shapes and portal sizes in the three **Mcp** crystal structures, we compared the following values: a) Atom separation distance across the cavity portals shown in Table 2 (C1–C68, C14–C61, C77–N4, with numbering as demonstrated in Fig. 1), b) Displacement of the metal ion from the least-square plane defined by the four porphyrin nitrogen atoms shown in Table 2, and c) Distortions of porphyrin planes shown in Fig. 3. The first conclusion is that the atom separation distances across the cavity portals are 3.4 to 4.2 Å. The fact that large differences among these values were not observed indicates that the **Mcp** portals are almost closed, and encapsulated guests cannot undergo fast exchange with guests outside of the cavity. Next, displacement distances of the metals out of the porphyrin plane for **Nicip** and **Pdcp** are essentially zero. On the other hand, the Zn ions in **Zntpp** and **Zncp** both lie about 0.2 Å above the planes toward the methanol and the cavitand. In general, Ni<sup>II</sup> and Pd<sup>II</sup> ion are

observed to favor four-coordinate square-planar geometry, while the Zn<sup>II</sup> ion favors five-coordinate square pyramidal geometry. In the crystal structure of [Zncp(MeOH)], the Zn ion is directed toward the cavity side, because of favorable fit of MeOH to the cavity. In addition, we evaluated the distortions of porphyrin planes of **Mcps** by measurement of the deviation of porphyrin-ring carbon atoms to the least-square planes based on porphyrin four nitrogen atoms.<sup>42</sup> The most distorted positions C2, C3, C7, and C8 are located near the cavitand linker in all **Mcps**, and their distortion values are within 0.3 Å. There are smaller values in comparison with the values among **Zntpp**, **Nitpp**, and **Pdtp**, respectively.<sup>43,44</sup> The decrease of porphyrin plane distortions will be dominantly caused by the cavitand bridging between two porphyrin *meso*-aryl groups. The metal ion is expected to have a negligible effect. Indeed, all the three distance measurements suggest that the cavity and portal spaces are not affected by the identity of the metal ion.

The largest difference among the crystal structures of **Mcp** is observed with regard to the distances between the metal ion and the oxygen atom of methanol (Table 2). The Zn–O length for the encapsulated methanol **Zncp** complex is 2.253 Å, indicating that MeOH is coordinated to the Zn ion. On the other hand, the analogous distances observed in the **Nicip** and **Pdcp** structures are 3.27 and 3.37 Å, respectively, which are too long to indicate coordination of methanol to the metals. Thus, the metal ion has an appreciable effect on guest inclusion properties. It appears that selectivity for guest functional groups could be controlled or fine-tuned by alternate metals incorporated into a standard **cp** host.

**Hydrocarbon Encapsulation into **Mcp**.** Our preliminary investigations<sup>27</sup> of small hydrocarbon encapsulation in free-base cavitand porphyrins led us to consider studies of corresponding metal derivatives (**Mcps**), because the character of a central metal ion could cooperatively function as a molecular recognition component. By choosing an appropriate metal ion, one can tune the recognition property of **Mcp**.

The ability of methane to function as a guest molecule was investigated. Methane gas was bubbled into the solution of **Zncp**, the resulting <sup>1</sup>H NMR spectrum in CDCl<sub>3</sub> is shown in Figs. 4A and 4B. A new signal at the extreme upfield region (as a singlet at –7.18 ppm) appeared as well as signals arising from **Zncp** and free methane. In addition, all signals of **Zncp** were split slightly by the addition of methane. When <sup>13</sup>CH<sub>4</sub> gas was bubbled into the solution of **Zncp**, <sup>1</sup>H and <sup>13</sup>C NMR spectra were recorded. In the <sup>1</sup>H NMR spectrum, the signal at –7.18 ppm was split to a doublet (*J* = 126 Hz). The coupling constant of the doublet was found to be typical of <sup>13</sup>C–<sup>1</sup>H spin coupling. In the <sup>13</sup>C NMR spectrum, a signal at –14.3 ppm appeared beside the signal from <sup>13</sup>CH<sub>4</sub>.<sup>45</sup> These signals disappeared when Ar gas was bubbled into the saturated methane solution. Based on these results, the signals were assigned to methane within the **Zncp** cavity since methane would be strongly shielded by the ring current of porphyrin and the cavitand aromatic rings.<sup>46–48</sup> Since this high field shift of methane was not observed in the experiment with **1**, **8**, or **Zntpp**, it was concluded that methane is encapsulated within the **Zncp** cavity. The guest exchange rate was slow enough to observe encapsulation by the <sup>1</sup>H and <sup>13</sup>C NMR. The relatively slow exchange

rate can be attributed to steric hindrance at the portal of the cavity and the energy barrier of its open form.

Zn $\text{cp}$  also demonstrates guest encapsulation of other small hydrocarbons (Fig. 4). These experiment were carried out

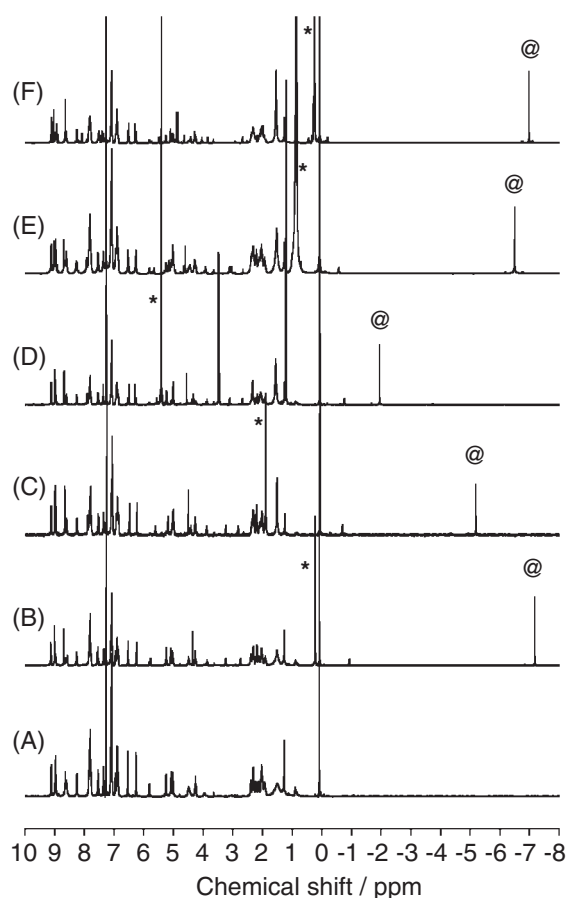


Fig. 4.  $^1\text{H}$ NMR spectra of (A) Zn $\text{cp}$ , (B) Zn $\text{cp}$  with methanol, (C) with acetylene, (D) with ethylene, (E) with ethane, and (F) with cyclopropane. \*: free guests, @: encapsulated guests.

using the four Mcps and hydrocarbons smaller than propane. The  $^1\text{H}$ NMR chemical shifts of encapsulated guests are shown in Table 3 ( $^1\text{H}$ NMR spectra of the free Mcps, and various guests with Mcps are included in the Supporting Information). All Mcps demonstrate encapsulation of smaller hydrocarbons including cyclopropane but not including propane. The limit of guest hydrocarbon molecules encapsulated into the Mcp cavities was found to be the cyclic  $\text{C}_3$  molecules. The shift magnitudes between free and encapsulated guest proton signals changed  $-6.5$  (Ni $\text{cp}$ ) to  $-7.5$  ( $\text{H}_2\text{cp}$  and Zn $\text{cp}$ ) ppm depending upon the metal species, and were not affected by the identity of the guest molecule. All encapsulated guest concentrations calculated from NMR signal intensities were smaller than that of the hosts. This suggests that only a single guest molecule is encapsulated by the cavity.

Chloroform, the solvent employed in all experiments, is larger than propane and its encapsulated signals were not observed in NMR experiments, indicating that it is not encapsulated.

**Coordinating Guest Encapsulation into Mcp.** Ten equivalents of methanol were added to the  $\text{CDCl}_3$  solution of Zn $\text{cp}$ , before measurement of  $^1\text{H}$ NMR spectra (Fig. 5D). Two new signals appeared at the extreme upfield region. Other signals arising from Zn $\text{cp}$  and free methanol are: a doublet at  $-3.77$  ppm ( $J = 5.1$  Hz;  $\text{CH}_3$ ) and a quartet at  $-7.11$  ppm ( $J = 5.1$  Hz; OH) in an integration ratio 3:1. Thus, Zn $\text{cp}$  encapsulated single MeOH molecule. The assignment was also confirmed by  $\text{CD}_3\text{OD}$ . The signals from Zn $\text{cp}$  were shifted slightly after addition of methanol. The encapsulation of a single MeOH molecule in the cavity is also observed in the crystal structure of [Zn $\text{cp}$ (MeOH)], which has a methanol molecule coordinated to Zn. The extreme upfield shifts of these two signals could be interpreted as resulting from a shielding effect derived from the ring current of the porphyrin and the aromatic rings of the cavitand. The OH proton signal of the encapsulated methanol in Zn $\text{cp}$  is a sharp quartet coupled to the neighboring methyl group. In contrast, fast proton exchange occurring in bulk solution tends to broaden the signal. These results suggest that the methanol molecule within the cp cavity is not capable of

Table 3.  $^1\text{H}$ NMR Data of the Encapsulated Guests in Mcps<sup>a)</sup>

Guest	Free	$\text{H}_2\text{cp}$	Ni $\text{cp}$	Zn $\text{cp}$	Pd $\text{cp}$
Methane	0.15	$-7.19$	$-6.26$	$-7.18$	$-6.96$
Acetylene	1.91	$-5.37$	$-4.59$	$-5.17$	$-4.84$
Ethylene	5.39	$-2.07$	$-1.19$	$-1.95$	$-1.68$
Ethane	0.85	$-6.49$	$-5.48$	$-6.50$	$-6.12$
Cyclopropane	0.23	$-6.95$	$-5.84$	$-6.99$	$-6.45$
Propane	1.31 ( $\text{CH}_2$ ) 0.88 ( $\text{CH}_3$ )	— <sup>b)</sup>	— <sup>b)</sup>	— <sup>b)</sup>	— <sup>b)</sup>
MeOH	3.39 ( $\text{CH}_3$ )	$-3.71$ (d, $J = 5.1$ , $\text{CH}_3$ ) $-7.21$ (q, $J = 5.1$ , OH)	$-3.10$ (br, $\text{CH}_3$ ) $-6.16$ (br, OH)	$-3.72$ (d, $J = 5.1$ , $\text{CH}_3$ ) $-7.11$ (q, $J = 5.1$ , OH)	$-3.65$ (d, $J = 5.6$ , $\text{CH}_3$ ) $-7.04$ (q, $J = 5.6$ , OH)
EtOH	3.64 (q, $J = 7.1$ , $\text{CH}_2$ ) 1.17 (t, $J = 7.1$ , $\text{CH}_3$ )	$-4.02$ (br, $\text{CH}_2$ ) $-5.70$ (br, $\text{CH}_3$ ) $-6.86$ (br, OH)	— <sup>b)</sup>	$-3.94$ (m, $\text{CH}_2$ ) $-5.47$ (t, $J = 7.3$ , $\text{CH}_3$ ) $-6.86$ (t, $J = 5.6$ , OH)	— <sup>b)</sup>
MeCN	1.98	— <sup>b)</sup>	— <sup>b)</sup>	$-4.29$	— <sup>b)</sup>

a) [Mcp] = 5 mM, at 25 °C in  $\text{CDCl}_3$ . Chemical shifts are based on TMS. All signals without indication of their multiplicity are singlet. b) Not encapsulated.

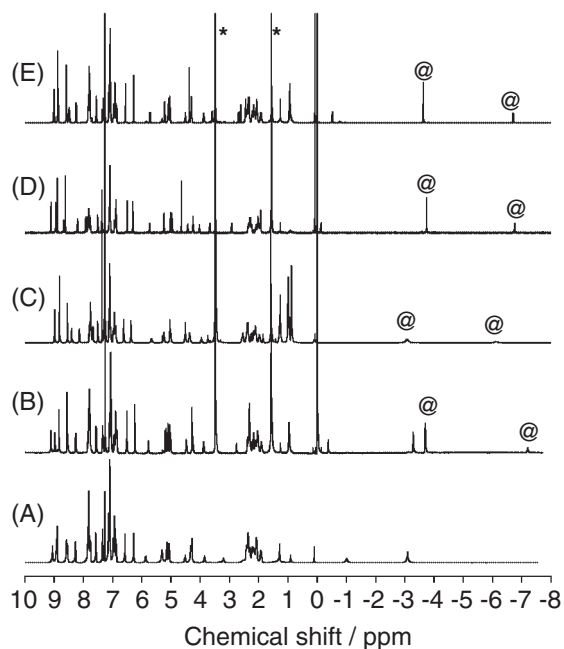


Fig. 5.  $^1\text{H}$ NMR spectra of (A)  $\text{H}_2\text{cp}$ , (B)  $\text{H}_2\text{cp}$  with MeOH, (C)  $\text{Ni}\text{cp}$  with MeOH, (D)  $\text{Zn}\text{cp}$  with MeOH, and (E)  $\text{Pd}\text{cp}$  with MeOH. \*: free MeOH, @: encapsulated MeOH.

fast proton exchange with solvent protons within the NMR time scale.

The encapsulated methanol is observed in the presence of other  $\text{Mcp}$  hosts (shown in Fig. 5 and Table 3). Ethanol and acetonitrile are also encapsulated in the  $\text{Mcp}$  cavities as confirmed by  $^1\text{H}$ NMR measurements (shown in Supporting Information). The encapsulation properties of these two guests depend on the metal ions. The encapsulated ethanol signals were observed in  $\text{H}_2\text{cp}$  (at  $-4.02$ ,  $-5.70$ ,  $-6.86$  ppm) and  $\text{Zncp}$  (at  $-3.94$ ,  $-5.47$ ,  $-6.86$  ppm).  $\text{Ni}\text{cp}$  and  $\text{Pdcp}$  did not encapsulate these guests. Acetonitrile was also only encapsulated by  $\text{Zncp}$  (signal at  $-4.29$  ppm) but not in  $\text{Ni}\text{cp}$  and  $\text{Pdcp}$ . In all encapsulated guests examined, the signals of encapsulated guests shifted  $-6$ – $-7$  ppm from the signals of the free guests and exchange rates of the guests were slow enough to detect the encapsulation of the guest by  $^1\text{H}$ NMR spectroscopy.

The size of the encapsulated molecules shows interesting features. For hydrocarbons, cyclopropane, a cyclic  $\text{C}_3$  molecule, is the largest molecule to be encapsulated, and propane, a linear  $\text{C}_3$  molecule is too large to be encapsulated. However, some larger linear guest molecules with coordinating functional groups can be encapsulated by  $\text{H}_2$ - and  $\text{Zncp}$  ( $\text{H}_2\text{cp}$  with ethanol,  $\text{Zncp}$  with ethanol or acetonitrile). Rebek and Mecozzi defined packing coefficient (PC) as the ratio of the guest volume to the host one and reported its moderate value is  $55 \pm 0.09\%$  in solution.<sup>49</sup> In the present instances, PC values for hydrocarbons, non-polar guests, in the  $\text{cp}$  cavity (volume  $83 \text{ \AA}^3$ ) range from 29 (methane) to 57% (cyclopropane) (Fig. S2). These results show moderate correlation with other hosts, which do not have any strong interaction with guests. When one uses host–guest systems showing strong interaction, this empirical rule fails:  $\text{H}_2\text{cp}$  and  $\text{Zncp}$  can encapsulate large molecules such as EtOH (PC 86%). Hydrogen bonding or

Table 4. The Binding Constants  $K_{11}$  ( $\text{M}^{-1}$ ) of Various Guests in  $\text{Mcp}$ s ( $\text{M} = \text{H}_2, \text{Ni}, \text{Zn}, \text{and Pd}$ ) Determined by  $^1\text{H}$ NMR<sup>a)</sup>

	$\text{H}_2\text{cp}$	$\text{Ni}\text{cp}$	$\text{Zncp}^{\text{b)}$	$\text{Pdcp}$
Methane	$81 \pm 18$	$150 \pm 10$	57	$150 \pm 10$
Acetylene	$130 \pm 20$	$130 \pm 10$	130	$130 \pm 10$
Ethylene	$49 \pm 5$	$65 \pm 5$	37	$53 \pm 3$
Ethane	$9.4 \pm 1.4$	$7.5 \pm 0.5$	4.9	$7.1 \pm 0.3$
Cyclopropane	$9.6 \pm 2.3$	$2.1 \pm 0.3$	9.9	$1.3 \pm 0.2$
MeOH	$240 \pm 10$	$70 \pm 5$	$>40000^{\text{c)}$	$94 \pm 5$
EtOH	$3.8 \pm 1.6$	— <sup>d)</sup>	1100	— <sup>d)</sup>
MeCN	— <sup>d)</sup>	— <sup>d)</sup>	68	— <sup>d)</sup>

a)  $[\text{Mcp}] = 5 \text{ mM}$ , at  $25^\circ\text{C}$  in  $\text{CDCl}_3$ . b) Apparent  $K_{11}$  calculated by Eq. 1 (see, Experimental) assuming  $[\text{H}_2\text{O}] \approx 10$ – $20 \text{ mM}$ . c) Observed by UV–vis titration. d) Not encapsulated.

coordination between free-base/ $\text{Zn}$  porphyrins and the guest molecules enhance encapsulation affinity, presumably because the short guest–porphyrin distance allows trapping of larger guests. Thus, so-called 55%-rule holds only in host–guest combinations, where any strong interactions do not exist, and strongly interacting host–guest combination will allow larger PC values by its compact packing.

Water is a typical polar coordinating solvent, which would be expected to coordinate to  $\text{Mcp}$ . However,  $^1\text{H}$ NMR spectra of  $\text{CDCl}_3$  solutions (without drying) showed no proton signals corresponding to encapsulated water molecules. This can be explained by the fast exchange of the coordinated water molecule(s) in the  $\text{Mcp}$  cavities with outside water molecules, which occurs through the  $\text{Mcp}$  portal at a rate faster than the NMR timescale. Determination of water encapsulation by  $\text{Mcp}$ s is described in the following section.

**Binding Constants of Guest Encapsulation in  $\text{Mcp}$ .** To inspect the guest selectivity both to  $\text{Mcp}$  cavity sizes and to the difference of the metal ions in the porphyrins, the binding constants  $K_{11}$  of the guest encapsulations in  $\text{Mcp}$ s were determined by  $^1\text{H}$ NMR titrations, and are shown in Table 4 (In the case of  $\text{Zncp}$ , the binding constants are mentioned below). At first, we focus the effect of metal insertion on guest encapsulation by comparing  $K_{11}$  values for hydrocarbons binding to  $\text{H}_2\text{cp}$  and to  $\text{Ni}\text{cp}$ . The  $K_{11}$  values of methane and methanol (smaller guests examined) for  $\text{Ni}\text{cp}$  are larger than the corresponding values for  $\text{H}_2\text{cp}$ . In contrast, the  $K_{11}$  values of ethane and ethanol encapsulation in  $\text{Ni}\text{cp}$  are smaller than the values for  $\text{H}_2\text{cp}$ . Furthermore, the  $K_{11}$  value of acetylene in  $\text{H}_2\text{cp}$  is the largest among values of all examined hydrocarbons and the  $K_{11}$  value of methane is the largest in  $\text{Ni}\text{cp}$ . This indicates that  $\text{Ni}\text{cp}$  favors smaller guests than  $\text{H}_2\text{cp}$ . Since the  $K_{11}$  values for each guest molecule binding to  $\text{Ni}\text{cp}$  shows close similarities to the analogous  $K_{11}$  values for  $\text{Pdcp}$ , the differences in metal ion radius from Ni to Pd appears to have no effect on guest binding. The decrease in porphyrin ring flexibility induced by metal insertion will have a considerable effect on guest size selectivity.

On the other hand, coordinating polar guest molecules show remarkable differences in encapsulation by  $\text{Mcp}$ s. Intrinsically,  $\text{Ni}^{\text{II}}$  favors four-coordinate square-planar geometry, while

Zn<sup>II</sup> prefers five-coordinate trigonal bipyramidal geometry. Since water acts as a ligand to Zn<sup>II</sup> complexes, the observed  $K_{11}$  values of methane to Zncp are greatly affected by the water concentration in the solvent. This effect is not observed for the other Mcps (Fig. 6). In consideration of the cavity volume of Mcp, the volume occupied by a water molecule cannot be ignored since the apparent  $K_{11}$  values for methane in Zncp decreased with increasing water concentrations. On the other hand, observed  $K_{11}$  values for H<sub>2</sub>cp, Nicp, and Pdcp were not affected by water concentration. This result coincides with the low affinity of water to H<sub>2</sub>cp, Nicp, and Pdcp.

As one would expect, Mcp metal ions have a major effect on encapsulation of polar molecules. The  $K_{11}$  values of alcohols show large differences, which depend upon the identity of the metal ion of Mcp.  $K_{11}$  value of methanol to Zntpp was reported to be  $\approx 9.6 \text{ M}^{-1}$  (in benzene, at 24 °C).<sup>50</sup> Methanol binding affinity of Zncp increases in  $\approx 4 \times 10^3$  times higher than that for Zntpp. These results clearly show that the capsule formation as cp has a remarkable effect on enhancement of the guest coordination by cooperation with the higher host affinity to Zncp.

$K_{11}$  values of methanol encapsulation within Nicp and Pdcp

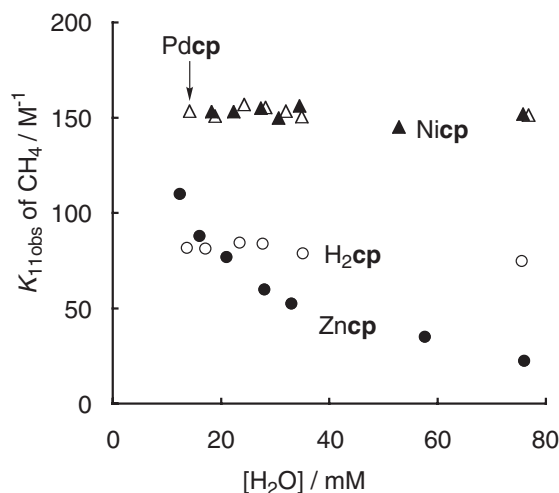


Fig. 6. Effect of water concentration on  $K_{11\text{obs}}$  of methane encapsulation in Mcp (M = H<sub>2</sub>, Ni, Zn, and Pd) observed by <sup>1</sup>H NMR. [Mcp] = 5 mM, [CH<sub>4</sub>]  $\approx$  10 mM at 25 °C in CDCl<sub>3</sub>.

were almost within the same range as the values measured for encapsulation of hydrocarbons. In consideration of the character of both metal ions, the van der Waals interaction is the major and dominant interaction between the guest and the host. However, since H<sub>2</sub>cp as well as Zncp, methanol can take H-bonding interaction with the four N atoms of the free-base porphyrin, a higher  $K_{11}$  value for encapsulation of methanol was observed than for Nicp and Pdcp. EtOH has remarkably smaller  $K_{11}$  values in Mcps, presumably because of its larger size. Acetonitrile was only encapsulated in Zncp. From these results, it is surmised that the coordination guest selectivity is greatly affected by the coordinating ability of metals in Mcps, while the guest size selectivity is dominated by the host cavity size and is not affected by metal ions.

**Thermodynamic Parameters of Guest Encapsulation in Mcp.** Many reports of small hydrocarbon encapsulations in capsule-shaped hosts have been made. However, there have been very few investigations of the intrinsic thermodynamic parameters of the reported systems.<sup>11,13,23</sup> For example, structurally rigid hosts, such as carcerands, inhibit guest exchange, and flexible or self-assembling hosts, must accommodate transient structural changes of host capsules. Mcps are suitable for these investigations (Table 5), because their structures contain two rigid components linked by flexible joints, which can moderate guest exchange rates.  $\Delta G^\circ$  and  $\Delta H^\circ$  values were calculated from  $K_{11}$  values at 25 °C and by van't Hoff plots with  $K_{11}$  values, respectively, between 25 and 45 °C in CDCl<sub>3</sub>.

All of the measurements of  $\Delta G^\circ$ ,  $\Delta H^\circ$ , and  $\Delta S^\circ$  for the small guest–Mcp systems had negative values. A negative  $\Delta H^\circ$  indicates that the encapsulation of guests is favorable. On the other hand, a negative  $\Delta S^\circ$  value indicates that encapsulation is disadvantageous due to the loss of guest translational freedom. Consequently, the inclusion of guests in Mcp cavities is dominated by larger enthalpic gains than is offset by entropic losses. Detailed interpretation of relative  $\Delta H^\circ$  and  $\Delta S^\circ$  values is not appropriate due to the large intrinsic error arising from the <sup>1</sup>H NMR integration process.

Our results are comparable with those observed for Rebek's "tennis ball" capsule<sup>11</sup> (for methane:  $K = 300 \text{ M}^{-1}$  (at 273 K),  $\Delta H^\circ = -38 \text{ kJ mol}^{-1}$ ,  $\Delta S^\circ = -84 \text{ J K}^{-1} \text{ mol}^{-1}$ ; for ethylene:  $K = 280 \text{ M}^{-1}$  (at 273 K),  $\Delta H^\circ = -38 \text{ kJ mol}^{-1}$ ,  $\Delta S^\circ = -125 \text{ J K}^{-1} \text{ mol}^{-1}$ , in CDCl<sub>3</sub>). This suggests that both systems have similar dynamic properties of host structures for guest stabilization as well as similar cavity sizes.

Table 5. Thermodynamic Parameters of Various Guests in Mcps (M = H<sub>2</sub>, Ni, and Pd) observed by <sup>1</sup>H NMR<sup>a)</sup>

Guest	H <sub>2</sub> cp			Nicp			Pdcp		
	$\Delta G^\circ$ /kJ mol <sup>-1</sup>	$\Delta H^\circ$ <sup>b)</sup> /kJ mol <sup>-1</sup>	$\Delta S^\circ$ <sup>b)</sup> /J K <sup>-1</sup> mol <sup>-1</sup>	$\Delta G^\circ$ /kJ mol <sup>-1</sup>	$\Delta H^\circ$ <sup>b)</sup> /kJ mol <sup>-1</sup>	$\Delta S^\circ$ <sup>b)</sup> /J K <sup>-1</sup> mol <sup>-1</sup>	$\Delta G^\circ$ /kJ mol <sup>-1</sup>	$\Delta H^\circ$ <sup>b)</sup> /kJ mol <sup>-1</sup>	$\Delta S^\circ$ <sup>b)</sup> /J K <sup>-1</sup> mol <sup>-1</sup>
Methane	-10.9	-33	-75	-12.4	-25	-43	-12.4	-32	-67
Acetylene	-12.1	-33	-71	-12.0	-33	-71	-12.0	-32	-66
Ethylene	-9.7	-29	-66	-10.3	-36	-84	-9.8	-32	-74
Ethane	-5.5	-36	-100	-5.0	-36	-100	-4.8	-35	-100
Cyclopropane	-5.6	-30	-82	— <sup>c)</sup>	— <sup>c)</sup>	— <sup>c)</sup>	— <sup>c)</sup>	— <sup>c)</sup>	— <sup>c)</sup>
MeOH	-13.5	-32	-62	-10.5	-27	-55	-11.2	-24	-43
EtOH	-3.29	-39	-120	— <sup>d)</sup>	— <sup>d)</sup>	— <sup>d)</sup>	— <sup>d)</sup>	— <sup>d)</sup>	— <sup>d)</sup>

a) [Mcp] = 5 mM, at 25–45 °C in CDCl<sub>3</sub>. b) Errors were estimated to be within  $\pm 20\%$  mainly due to integration of the <sup>1</sup>H NMR spectra. c) Not determined. d) Not encapsulated.

## Conclusion

A series of new host “cavitand–porphyrin” metal complexes **Mcp** (M = H<sub>2</sub>, Ni, Zn, and Pd) which have small cavities. The crystal structures of cavitand **1**, **Zntpp**(MeOH), and **Mcps** (M = Zn, Ni, and Pd) have been solved and compared. One methanol molecule, originating from crystallization solvent is encapsulated in each host cavity, and coordinates to Zn in **Zncp** but not in Ni- and **Pdcp**. Analyses of distortions of the porphyrin planes, cavity portal sizes, and the distances of the metals to the porphyrin planes indicate that the size and shape of the **Mcp** cavities and portals are not affected by the metal ion in each of the porphyrins.

Encapsulation of various guest molecules in **Mcps** was confirmed by <sup>1</sup>H NMR. Among the hydrocarbon molecules investigated, methane, acetylene, ethylene, ethane, and cyclopropane were encapsulated. Proton signals of encapsulated guests appear at an upfield region shifted about –7 ppm due to slow guest-exchange rates and strong shielding by the aromatic wall of the cavitand and the porphyrin ring current. The binding constants of methane and acetylene in the **Mcp** cavities are the largest among the hydrocarbon guest molecules. Introduction of the metal ions (Ni and Pd) into the porphyrin of **H<sub>2</sub>cp** slightly affects guest encapsulation in favor of smaller guest molecule sizes. While the difference of metal ion radius between Ni and Pd did not have an appreciable effect on guest binding, the decrease of porphyrin ring flexibility induced by metal insertion does have a considerable effect on guest size selectivity.

Methanol, ethanol, and acetonitrile are all encapsulated by **Mcps**. Solvent-originating methanol was encapsulated in all **Mcp** cavities as shown in the crystal structures. Ethanol is encapsulated in **H<sub>2</sub>cp** and **Zncp**. Acetonitrile is only encapsulated in **Zncp**. These results indicate that the encapsulation dynamics for coordination of guests in the **Mcp** cavities could be changed by changing the metal ion species in the porphyrin. Water and alcohol ligands can coordinate to **Zncp** and the coordinated water also affects methane binding to **Zncp** as evidenced by competition experiments of methane with water in **Mcp**. The other **Mcps** have only slight affinity for water, if any.

Calculations of thermodynamic parameters of all guest encapsulations in **Mcp** indicate that this inclusion phenomenon is dominated by larger enthalpic gains than offset by entropic losses.

It was confirmed that the new host compounds **Mcps** are capable of size selective encapsulation of small guest molecules. We demonstrated that encapsulation properties of the **Mcps** can be tuned by metal ions in the porphyrin center. Introduction of redox active metal ions such as iron, manganese, and ruthenium into **H<sub>2</sub>cp** may provide oxidation catalysts, for oxidation of small hydrocarbons. Further study is in progress on this line.

## Experimental

**Materials and Instruments.** Commercially available reagents and solvents were used without further purification unless otherwise noted. Tetrahydrofuran (THF) was dried over KOH, and distilled from sodium diphenylketyl under N<sub>2</sub> atmosphere. Dichloro-

methane was stirred with concd H<sub>2</sub>SO<sub>4</sub> for several days, neutralized with K<sub>2</sub>CO<sub>3</sub> and then distilled from CaH<sub>2</sub> under N<sub>2</sub> atmosphere. *N,N*-Dimethylformamide (DMF) was distilled from CaH<sub>2</sub> under reduced pressure and dried over molecular sieves 4A. *N*-Methylpyrrolidone (NMP) was dried over molecular sieves 4A for several days. Dimethyl sulfoxide (DMSO) was distilled from CaH<sub>2</sub> under reduced pressure. Me<sub>2</sub>S was distilled and dried over molecular sieves 4A. Pyrrole was distilled under reduced pressure. CDCl<sub>3</sub> (99.8 atom % D, ACROS ORGANICS) was passed through an alumina column to remove an acid.

<sup>1</sup>H and <sup>13</sup>C NMR spectra were recorded on a JEOL JMX-GX400 (400 MHz) spectrometer. Chemical shifts were reported on  $\delta$ -scale relative to tetramethylsilane (TMS). High-resolution MS (HR-MS) spectra were recorded on a JEOL LMS-HX-110 spectrometer. FAB-MS spectra were measured with 3-nitrobenzyl alcohol (NBA) as matrix. UV–vis absorption spectra were recorded on a Shimadzu UV-3100PC spectrophotometer.

**Mcp Synthesis.** Cavitand (**1**; 2,3-dihydro-1,21,23,25-tetrakis(2-phenylethyl)-2,20:3,19-dimetheno-1*H*,21*H*,23*H*,25*H*-bis[1,3]-dioxocino[5,4-*i*:5',4'-*i'*]benzo[1,2-*d*:5,4-*d'*]bis[1,3]benzodioxocin) and dibromocavitand (**2**; 7,11-dibromo-2,3-dihydro-1,21,23,25-tetrakis(2-phenylethyl)-2,20:3,19-dimetheno-1*H*,21*H*,23*H*,25*H*-bis[1,3]dioxocino[5,4-*i*:5',4'-*i'*]benzo[1,2-*d*:5,4-*d'*]bis[1,3]benzodioxocin) were synthesized according to literatures.<sup>30,39</sup>

**Diformylcavitand (3; 2,3-Dihydro-1,21,23,25-tetrakis(2-phenylethyl)-2,20:3,19-dimetheno-1*H*,21*H*,23*H*,25*H*-bis[1,3]dioxocino[5,4-*i*:5',4'-*i'*]benzo[1,2-*d*:5,4-*d'*]bis[1,3]benzodioxocin-7,11-dicarbaldehyde):** To a solution of **2** (1.11 g, 1.00 mmol) in dry THF (100 mL) at –78 °C under N<sub>2</sub> was quickly added 1.6 M hexane solution of *n*-BuLi (2.0 mL, 3.2 mmol). After 1 min, excess amount of dry DMF (1.0 mL) was added to the reaction mixture, which was allowed to room temperature and further stirred overnight, then quenched with water. THF was evaporated and the residue was extracted by CH<sub>2</sub>Cl<sub>2</sub>. The organic layer was washed with 1 M HCl, water (×3), and brine, dried with Na<sub>2</sub>SO<sub>4</sub>, and then evaporated. The residue was purified by silica-gel column chromatography (CH<sub>2</sub>Cl<sub>2</sub>–AcOEt = 20:1 v/v) to give **3** as a white solid in 47% yield (473 mg, 469  $\mu$ mol) and monoformylcavitand as a by-product. The product was dried in vacuo at 120 °C for 3 h, prior to the next reaction.

**3:** mp 176–178 °C. <sup>1</sup>H NMR (400 MHz, CDCl<sub>3</sub>):  $\delta$  10.28 (s, 2H, CHO), 7.35–7.12 (m, 24H, CHCH<sub>2</sub>CH<sub>2</sub>C<sub>6</sub>H<sub>5</sub> + Ar–H *meta* to OCH<sub>2</sub>O), 6.58 (s, 2H, Ar–H *ortho* to OCH<sub>2</sub>O), 5.92 (d, *J* = 7.6 Hz, 1H, H<sub>ao</sub> of OCH<sub>2</sub>O), 5.77 (d, *J* = 7.2 Hz, 1H, H<sub>co</sub> of OCH<sub>2</sub>O), 5.54 (d, *J* = 7.2 Hz, 2H, H<sub>bo</sub> of OCH<sub>2</sub>O), 5.00 (t, *J* = 8.0 Hz, 1H, CHCH<sub>2</sub>CH<sub>2</sub>C<sub>6</sub>H<sub>5</sub>), 4.92 (t, *J* = 8.0 Hz, 2H, CHCH<sub>2</sub>CH<sub>2</sub>C<sub>6</sub>H<sub>5</sub>), 4.85 (t, *J* = 7.6 Hz, 1H, CHCH<sub>2</sub>CH<sub>2</sub>C<sub>6</sub>H<sub>5</sub>), 4.50–4.46 (m, 4H, H<sub>ai</sub>, H<sub>bi</sub>, and H<sub>ci</sub> of OCH<sub>2</sub>O), 2.69–2.53 (m, 16H, CHCH<sub>2</sub>CH<sub>2</sub>C<sub>6</sub>H<sub>5</sub>). HR-MS (C<sub>66</sub>H<sub>57</sub>O<sub>10</sub>): *m/z* = calcd 1009.3952, found 1009.3954.

**Bis(hydroxymethyl)cavitand (4; 7,11-Bis(hydroxymethyl)-2,3-dihydro-1,21,23,25-tetrakis(2-phenylethyl)-2,20:3,19-dimetheno-1*H*,21*H*,23*H*,25*H*-bis[1,3]dioxocino[5,4-*i*:5',4'-*i'*]benzo[1,2-*d*:5,4-*d'*]bis[1,3]benzodioxocin):** To a suspension of LiAlH<sub>4</sub> (1.17 mg) in dry THF (20 mL) at 0 °C under N<sub>2</sub> was added dropwise the solution of **3** (473 mg, 469  $\mu$ mol) in dry THF (100 mL) for 30 min. The reaction mixture was allowed to room temperature and further stirred for 1 h. It was then carefully quenched with ice water. After THF was evaporated, the residue was extracted by CH<sub>2</sub>Cl<sub>2</sub>. The organic layer was washed with 1 M HCl, water (×3), and brine, dried with Na<sub>2</sub>SO<sub>4</sub>, and then evaporated. The residue was purified by silica-gel column chro-

matography (CH<sub>2</sub>Cl<sub>2</sub>-AcOEt = 2:1 v/v) to give **4** as a white solid in 98% yield (467 mg, 461 μmol). The product was dried in vacuo at 120 °C for 3 h, prior to the next reaction.

**4**: mp 243–247 °C. <sup>1</sup>H NMR (400 MHz, CDCl<sub>3</sub>): δ 7.23–7.15 (m, 24H, CHCH<sub>2</sub>CH<sub>2</sub>C<sub>6</sub>H<sub>5</sub> + Ar-H *meta* to OCH<sub>2</sub>O), 6.57 (s, 2H, Ar-H *ortho* to OCH<sub>2</sub>O), 5.94 (d, *J* = 6.8 Hz, 1H, H<sub>ao</sub> of OCH<sub>2</sub>O), 5.84 (d, *J* = 6.8 Hz, 2H, H<sub>bo</sub> of OCH<sub>2</sub>O), 5.74 (d, *J* = 7.2 Hz, 1H, H<sub>co</sub> of OCH<sub>2</sub>O), 4.90–4.86 (m, 4H, CHCH<sub>2</sub>CH<sub>2</sub>C<sub>6</sub>H<sub>5</sub>), 4.61–4.59 (s + d, 5H, *J* = 6.8 Hz, ArCH<sub>2</sub>OH, H<sub>ai</sub> of OCH<sub>2</sub>O), 4.48 (d, *J* = 7.6 Hz, 2H, H<sub>bi</sub> of OCH<sub>2</sub>O), 4.37 (d, *J* = 7.2 Hz, 1H, H<sub>ci</sub> of OCH<sub>2</sub>O), 2.70–2.52 (m, 16H, CHCH<sub>2</sub>CH<sub>2</sub>C<sub>6</sub>H<sub>5</sub>), 1.94 (t, *J* = 4.8 Hz, 2H, OH). HR-MS (C<sub>66</sub>H<sub>60</sub>O<sub>10</sub>): *m/z* = calcd 1012.4186, found 1012.4189.

**Bis(chloromethyl)cavitand (5; 7,11-Bis(chloromethyl)-2,3-dihydro-1,21,23,25-tetrakis(2-phenylethyl)-2,20:3,19-dimetheno-1H,21H,23H,25H-bis[1,3]dioxocino[5,4-*i*:5',4'-*i'*]benzo[1,2-*d*:5,4-*d'*]bis[1,3]benzodioxocin)**: To a suspension of *N*-chlorosuccinimide (500 mg, 3.74 mmol) in dry CH<sub>2</sub>Cl<sub>2</sub> (20 mL) at –20 °C under N<sub>2</sub> was quickly added dry Me<sub>2</sub>S (0.50 mL). Then, the solution of **4** (626 mg, 618 μmol) in dry CH<sub>2</sub>Cl<sub>2</sub> (100 mL) was added dropwise for 1 h. After completion of the addition, the reaction mixture was warmed to 0 °C and stirred for 2 h. It was then carefully quenched with water and extracted by CH<sub>2</sub>Cl<sub>2</sub>. The organic layer was washed with brine, dried with Na<sub>2</sub>SO<sub>4</sub>, and then evaporated. The residue was purified by silica-gel column chromatography (CH<sub>2</sub>Cl<sub>2</sub>) to give **5** as a white solid in 72% yield (466 mg, 444 μmol). The product was dried in vacuo at 120 °C for 3 h.

**5**: mp 260–263 °C. <sup>1</sup>H NMR (400 MHz, CDCl<sub>3</sub>): δ 7.24–7.12 (m, 24H, CHCH<sub>2</sub>CH<sub>2</sub>C<sub>6</sub>H<sub>5</sub> + Ar-H *meta* to OCH<sub>2</sub>O), 6.59 (s, 2H, Ar-H *ortho* to OCH<sub>2</sub>O), 6.00 (d, *J* = 7.6 Hz, 1H, H<sub>ao</sub> of OCH<sub>2</sub>O), 5.83 (d, *J* = 8.0 Hz, 2H, H<sub>bo</sub> of OCH<sub>2</sub>O), 5.81 (d, *J* = 7.2 Hz, 2H, H<sub>co</sub> of OCH<sub>2</sub>O), 4.89–4.85 (m, 4H, CHCH<sub>2</sub>CH<sub>2</sub>C<sub>6</sub>H<sub>5</sub>), 4.73 (d, *J* = 7.6 Hz, 1H, H<sub>ai</sub> of OCH<sub>2</sub>O), 4.65 (s, 4H, ArCH<sub>2</sub>Cl), 4.63 (d, *J* = 7.2 Hz, 2H, H<sub>bi</sub> of OCH<sub>2</sub>O), 4.52 (d, *J* = 7.2 Hz, 1H, H<sub>ci</sub> of OCH<sub>2</sub>O), 2.69–2.51 (m, 16H, CHCH<sub>2</sub>CH<sub>2</sub>C<sub>6</sub>H<sub>5</sub>). HR-MS (C<sub>66</sub>H<sub>58</sub>Cl<sub>2</sub>O<sub>8</sub>): *m/z* = calcd 1048.3509, found 1048.3510.

**meso-Bis(2-methoxyphenyl)diphenylporphyrin Stereoisomeric Mixture (6)**: To the solution of benzaldehyde (35 mL, 336 mmol), 2-methoxybenzaldehyde (45.8 g, 336 mmol), and propionic anhydride (40 mL) in refluxing propionic acid (2000 mL) under aerobic conditions was slowly added pyrrole (44 mL, 640 mmol). The reaction mixture was stirred for 2 h and then evaporated. The residue was washed by MeOH and then purified by alumina-column chromatography (CHCl<sub>3</sub>) to give the mixture of tetraarylporphyrins, which were further separated carefully by silica-gel column chromatography (benzene). The fraction of dimethoxy porphyrin, which was eluted at third and fourth, was collected and evaporated to give **6** as a purple solid in 14.4% yield based on the amount of pyrrole (15.5 g, 23.0 mmol). The product was dried in vacuo at room temperature for 3 h prior to the next reaction.

**6**: <sup>1</sup>H NMR (400 MHz, CDCl<sub>3</sub>): δ 8.80–8.76 (m, 8H, pyrrole β-H), 8.22–8.18 (m, 4H, Ar-H), 8.02–7.97 (m, 2H, Ar-H), 7.77–7.70 (m, 8H, Ar-H), 7.36–7.31 (m, 4H, Ar-H), 3.59–3.55 (m, 6H, OCH<sub>3</sub>), –2.69 (s, 2H, NH). HR-MS (C<sub>46</sub>H<sub>34</sub>N<sub>4</sub>O<sub>2</sub>): *m/z* = calcd 674.2682, found 674.2671.

**meso-Bis(2-hydroxyphenyl)diphenylporphyrin (7) (as a stereoisomeric mixture)**: The mixture of **6** (153 mg, 227 μmol) and an excess amount of pyridinium hydrochloride was heated for 3 h at 240 °C under N<sub>2</sub>. Pyridinium salt melted and refluxed at the temperature. The reaction mixture was cooled to below 100 °C, and then treated with water. The residue was extracted with

chloroform washed with 1 M HCl, saturated solution of NaHCO<sub>3</sub> in water, and brine. The organic layer was dried with Na<sub>2</sub>SO<sub>4</sub>, and then evaporated, then purified by alumina-column chromatography (CHCl<sub>3</sub>). The first and second fractions were collected. The two fractions were combined and evaporated to give **7** as a purple solid in 89% yield (131 mg, 203 μmol). The product was dried in vacuo at 120 °C for 3 h.

**7**: <sup>1</sup>H NMR (400 MHz, CDCl<sub>3</sub>): δ 8.89–8.86 (m, 8H, pyrrole β-H), 8.21–8.19 (m, 4H, Ar-H), 8.01–7.96 (m, 2H, Ar-H), 7.81–7.69 (m, 8H, Ar-H), 7.36–7.31 (m, 4H, Ar-H), 4.98 (brs, 2H, OH), –2.75 (s, 2H, NH). HR-MS (C<sub>44</sub>H<sub>30</sub>N<sub>4</sub>O<sub>2</sub>): *m/z* = calcd 646.2369, found 646.2370.

**Cavitand-Porphyrin (H<sub>2</sub>cp) and Its Configurational Isomer (8)**: **5** (400 mg, 381 μmol), **7** (255 mg, 394 μmol), and K<sub>2</sub>CO<sub>3</sub> (1.0 g) were dried in vacuo at 120 °C with CaCl<sub>2</sub> for 3 h prior to the reaction. The mixture of **5**, **7**, and K<sub>2</sub>CO<sub>3</sub> in dry NMP (80 mL) and dry THF (80 mL) was heated for 4 days at 120 °C in an autoclave. After cooled to room temperature, THF was evaporated and the residue was extracted with CHCl<sub>3</sub>. The organic layer was washed with 1 M HCl, water (×3), and brine, dried with Na<sub>2</sub>SO<sub>4</sub>, and then evaporated. The residue was passed through an activated alumina-column (CH<sub>2</sub>Cl<sub>2</sub>) and the eluate was evaporated. The residue was carefully purified by silica-gel column chromatography (benzene) to give a purple solid of H<sub>2</sub>cp (less polar fraction) in 46% yield (286 mg, 176 μmol) and the configurational isomer **8** as a purple solid (more polar fraction) in 14% yield (87 mg, 54 μmol). The products were recrystallized from chloroform/methanol and dried in vacuo (0.1 torr) at 120 °C for 6 h.

**H<sub>2</sub>cp**: mp ≈280 °C (dec). <sup>1</sup>H NMR (400 MHz, CDCl<sub>3</sub>): δ 9.05 (s, 2H, pyrrole β-H), 8.91 (m, 4H, pyrrole β-H), 8.57 (s, 2H, pyrrole β-H), 8.54 (s, 2H, Ar-H of porphyrin), 8.27 (d, *J* = 6.4 Hz, 2H, Ar-H of porphyrin), 7.90–7.70 (m, 10H, Ar-H of porphyrin), 7.56 (d, *J* = 8.0 Hz, 2H, Ar-H of porphyrin), 7.33 (t, *J* = 7.4 Hz, 2H, Ar-H of porphyrin), 7.13–6.84 (m, 20H, CHCH<sub>2</sub>CH<sub>2</sub>C<sub>6</sub>H<sub>5</sub>), 6.57 (s, 2H, Ar-H), 6.25 (s, 2H, Ar-H), 5.86 (br, 1H, H<sub>co</sub> of OCH<sub>2</sub>O), 5.31 (br, 2H, H<sub>bo</sub> of OCH<sub>2</sub>O), 5.12 (d, *J* = 8.0 Hz, 2H, bridge ArCH<sub>2</sub>OAr), 5.04 (d, *J* = 8.4 Hz, 2H, bridge ArCH<sub>2</sub>OAr), 4.51 (br, 1H, CHCH<sub>2</sub>CH<sub>2</sub>C<sub>6</sub>H<sub>5</sub>), 4.27 (br, 4H, CHCH<sub>2</sub>CH<sub>2</sub>C<sub>6</sub>H<sub>5</sub> + Ar-H), 3.83 (br, 1H, CHCH<sub>2</sub>CH<sub>2</sub>C<sub>6</sub>H<sub>5</sub>), 3.18 (br, 1H, H<sub>ci</sub> of OCH<sub>2</sub>O), 2.43–1.81 (m, 19H, CHCH<sub>2</sub>CH<sub>2</sub>C<sub>6</sub>H<sub>5</sub> + H<sub>ao</sub> and H<sub>bi</sub> of OCH<sub>2</sub>O), –1.13 (br, 1H, H<sub>ai</sub> of OCH<sub>2</sub>O), –3.12 (s, 2H, NH). HR-MS (C<sub>110</sub>H<sub>86</sub>N<sub>4</sub>O<sub>10</sub>): *m/z* = calcd 1622.6344, found 1622.6339. Elemental analysis calcd for C<sub>110</sub>H<sub>86</sub>N<sub>4</sub>O<sub>10</sub>·H<sub>2</sub>O: C, 80.47; H, 5.40; N, 3.41%. Found: C, 80.74; H, 5.34; N, 3.64%.

**Isomer 8**: mp ≈290 °C (dec). <sup>1</sup>H NMR (400 MHz, CDCl<sub>3</sub>): δ 9.03 (d, *J* = 4.4 Hz, 2H, pyrrole β-H), 8.95 (d, *J* = 5.2 Hz, 2H, pyrrole β-H), 8.82 (s, 2H, pyrrole β-H), 8.57 (s, 2H, pyrrole β-H), 8.30 (d, *J* = 7.4 Hz, 2H, Ar-H of porphyrin), 8.23 (d, *J* = 7.5 Hz, 2H, Ar-H of porphyrin), 8.10–8.07 (m, 2H, Ar-H of porphyrin), 7.83–7.74 (m, 8H, Ar-H of porphyrin), 7.54 (d, *J* = 7.5 Hz, 2H, Ar-H of porphyrin), 7.50 (d, 2H, *J* = 8.0 Hz, Ar-H of porphyrin), 7.18–6.90 (m, 20H, CHCH<sub>2</sub>CH<sub>2</sub>C<sub>6</sub>H<sub>5</sub>), 6.70–6.65 (m, 6H, Ar-H), 6.21 (d, *J* = 6.8 Hz, 2H, H<sub>bo</sub> of OCH<sub>2</sub>O), 5.85 (d, *J* = 7.4 Hz, 1H, H<sub>ao</sub> of OCH<sub>2</sub>O), 4.99 (d, *J* = 7.2 Hz, 2H, H<sub>bi</sub> of OCH<sub>2</sub>O), 4.83–4.75 (m, 5H, H<sub>ai</sub> of OCH<sub>2</sub>O + CHCH<sub>2</sub>CH<sub>2</sub>C<sub>6</sub>H<sub>5</sub>), 4.51 (d, *J* = 8.8 Hz, 2H, bridge ArCH<sub>2</sub>OAr), 3.76 (d, *J* = 8.4 Hz, 2H, bridge ArCH<sub>2</sub>OAr), 2.63–2.29 (m, 16H, CHCH<sub>2</sub>CH<sub>2</sub>C<sub>6</sub>H<sub>5</sub>), 1.68 (d, *J* = 7.6 Hz, 1H, H<sub>co</sub> of OCH<sub>2</sub>O), –0.37 (d, *J* = 7.2 Hz, 1H, H<sub>ci</sub> of OCH<sub>2</sub>O), –2.60 (s, 2H, NH). HR-MS (C<sub>110</sub>H<sub>86</sub>N<sub>4</sub>O<sub>10</sub>): *m/z* = calcd 1622.6344, found 1622.6348. Elemental analysis: calcd for C<sub>110</sub>H<sub>86</sub>N<sub>4</sub>O<sub>10</sub>·2H<sub>2</sub>O: C, 79.59; H, 5.47; N, 3.38%. Found: C, 79.75; H, 5.32; N, 3.35%.

**Cavitand-Porphyrinatonicel(II) (Nicip):** Ni(OAc)<sub>2</sub>·4H<sub>2</sub>O (500 mg) and H<sub>2</sub>cp (50 mg, 31 μmol) were refluxed in DMF (20 mL) for 12 h. Water (100 mL) was added to the reaction mixture and then, red powder was collected by filtration. The residue was passed through an alumina-column (CH<sub>2</sub>Cl<sub>2</sub>) to give red powder. The product was dissolved in a small amount of chloroform and diffused in methanol to give red crystals of [Nicip]·MeOH·2CHCl<sub>3</sub>·3H<sub>2</sub>O in 68% yield (35 mg, 21 μmol). Prior to elemental analysis and spectroscopic characterization, the crystal was dried in vacuo (0.1 torr) at 120 °C for 6 h to give a red powder of Nicip.

**Nicip:** <sup>1</sup>H NMR (400 MHz, CDCl<sub>3</sub>): δ 8.98 (d, *J* = 4.6 Hz, 2H, pyrrole β-H), 8.83 (d, *J* = 4.6 Hz, 2H, pyrrole β-H), 8.81 (s, 2H, pyrrole β-H), 8.52 (s, 2H, pyrrole β-H), 8.40 (d, *J* = 5.9 Hz, 2H, Ar-H of porphyrin), 8.16 (d, *J* = 7.1 Hz, 2H, Ar-H of porphyrin), 7.81–7.72 (m, 8H, Ar-H of porphyrin), 7.64 (d, *J* = 7.1 Hz, 2H, Ar-H of porphyrin), 7.51 (d, *J* = 8.0 Hz, 2H, Ar-H of porphyrin), 7.28 (t, *J* = 7.2 Hz, 2H, Ar-H of porphyrin), 7.15–6.88 (m, 20H, CHCH<sub>2</sub>CH<sub>2</sub>C<sub>6</sub>H<sub>5</sub>), 6.63 (s, 2H, Ar-H), 6.37 (s, 2H, Ar-H), 5.80 (br, 1H, H<sub>co</sub> of OCH<sub>2</sub>O), 5.34 (br, 2H, H<sub>bo</sub> of OCH<sub>2</sub>O), 5.07 (br, 4H, bridge ArCH<sub>2</sub>OAr), 4.44 (br, 5H, CHCH<sub>2</sub>CH<sub>2</sub>C<sub>6</sub>H<sub>5</sub>, Ar-H), 3.96 (br, 1H, CHCH<sub>2</sub>CH<sub>2</sub>C<sub>6</sub>H<sub>5</sub>), 3.14 (br, 1H, H<sub>ci</sub> of OCH<sub>2</sub>O), 2.41 (br, 2H, H<sub>bi</sub> of OCH<sub>2</sub>O), 2.41–1.96 (m, 16H, CHCH<sub>2</sub>CH<sub>2</sub>C<sub>6</sub>H<sub>5</sub>), 2.39 (br, 1H, H<sub>ao</sub> of OCH<sub>2</sub>O), –0.12 (br, 1H, H<sub>ai</sub> of OCH<sub>2</sub>O). HR-MS (C<sub>110</sub>H<sub>84</sub>N<sub>4</sub>O<sub>10</sub>Ni): *m/z* = calcd 1678.5541, found 1678.5559. Elemental analysis: calcd for C<sub>110</sub>H<sub>84</sub>N<sub>4</sub>O<sub>10</sub>Ni·0.5H<sub>2</sub>O: C, 78.20; H, 5.07; N, 3.32%. Found: C, 78.21; H, 5.07; N, 3.60%.

**Cavitand-Porphyrinatonicel(II) (Zncp):** Zn(OAc)<sub>2</sub>·2H<sub>2</sub>O (0.35 g) and H<sub>2</sub>cp (104 mg, 64 μmol) were refluxed in acetic acid (20 mL) for 6 h. The solvent was then evaporated under reduced pressure and the residue was purified by alumina-column chromatography (CHCl<sub>3</sub>) to give red powder. The product was dissolved in small amount of chloroform and diffused in methanol to give a red crystal of [Zncp(MeOH)]·2CHCl<sub>3</sub>·3H<sub>2</sub>O in 70% yield (76 mg, 45 μmol). Prior to elemental analysis and spectroscopic characterization, the crystal was dried in vacuo (0.1 torr) at 120 °C for 6 h to give a red powder of Zncp.

**Zncp:** <sup>1</sup>H NMR (400 MHz, CDCl<sub>3</sub>): δ 9.11–8.89 (m, 6H, pyrrole β-H), 8.63–8.60 (m, 4H, Ar-H of porphyrin, pyrrole β-H), 8.25 (d, *J* = 6.1 Hz, 2H, Ar-H of porphyrin), 7.85–7.78 (m, 10H, Ar-H of porphyrin), 7.54 (d, *J* = 8.0 Hz, 2H, Ar-H of porphyrin), 7.34 (t, *J* = 7.3 Hz, 2H, Ar-H of porphyrin), 7.12–6.85 (m, 20H, CHCH<sub>2</sub>CH<sub>2</sub>C<sub>6</sub>H<sub>5</sub>), 6.53 (s, 2H, Ar-H), 6.25 (s, 2H, Ar-H), 5.81 (d, *J* = 7.6 Hz, 1H, H<sub>co</sub> of OCH<sub>2</sub>O), 5.27 (d, *J* = 7.5 Hz, 2H, H<sub>bo</sub> of OCH<sub>2</sub>O), 5.09 (d, *J* = 8.3 Hz, 2H, bridge ArCH<sub>2</sub>OAr), 5.01 (d, *J* = 8.3 Hz, 2H, bridge ArCH<sub>2</sub>OAr), 4.48 (t, *J* = 8.0 Hz, 1H, CHCH<sub>2</sub>CH<sub>2</sub>C<sub>6</sub>H<sub>5</sub>), 4.29 (br, 2H, Ar-H), 4.27 (t, *J* = 7.8 Hz, 2H, CHCH<sub>2</sub>CH<sub>2</sub>C<sub>6</sub>H<sub>5</sub>), 3.86 (t, *J* = 7.8 Hz, 1H, CHCH<sub>2</sub>CH<sub>2</sub>C<sub>6</sub>H<sub>5</sub>), 3.23 (d, *J* = 7.6 Hz, 1H, H<sub>ci</sub> of OCH<sub>2</sub>O), 2.65 (d, *J* = 7.3 Hz, 1H, H<sub>ao</sub> of OCH<sub>2</sub>O), 2.39 (d, *J* = 7.3 Hz, 2H, H<sub>bi</sub> of OCH<sub>2</sub>O), 2.38–1.90 (m, 16H, CHCH<sub>2</sub>CH<sub>2</sub>C<sub>6</sub>H<sub>5</sub>), –1.06 (d, *J* = 7.3 Hz, 1H, H<sub>ai</sub> of OCH<sub>2</sub>O). HR-MS (C<sub>110</sub>H<sub>84</sub>N<sub>4</sub>O<sub>10</sub>Zn): *m/z* = calcd 1684.5479, found 1684.5428. Elemental analysis calcd for C<sub>110</sub>H<sub>84</sub>N<sub>4</sub>O<sub>10</sub>Zn·H<sub>2</sub>O: C, 77.48; H, 5.08; N, 3.29%. Found: C, 77.83; H, 5.09; N, 3.45%.

**Cavitand-Porphyrinatopalladium(II) (Pdcp):** PdCl<sub>2</sub> (300 mg) and H<sub>2</sub>cp (50 mg, 31 μmol) were stirred in benzonitrile (20 mL) at 60 °C for 3 days. The solvent was then evaporated under reduced pressure and the residue was purified by alumina-column chromatography (CH<sub>2</sub>Cl<sub>2</sub>) to give orange powder. The product was dissolved in small amount of chloroform and diffused in

methanol to give an orange crystal of [Pdcp]·MeOH·2CHCl<sub>3</sub>·3H<sub>2</sub>O in 70% yield (37 mg, 22 μmol). Prior to elemental analysis and spectroscopic characterization, the crystal was dried in vacuo (0.1 torr) at 120 °C for 6 h to give an orange powder.

**Pdcp:** <sup>1</sup>H NMR (400 MHz, CDCl<sub>3</sub>): δ 8.99 (d, *J* = 4.9 Hz, 2H, pyrrole β-H), 8.85 (s + d, *J* = 3.7 Hz, 4H, pyrrole β-H), 8.56 (s, 2H, pyrrole β-H), 8.46 (d, *J* = 6.2 Hz, 2H, Ar-H of porphyrin), 8.24 (d, *J* = 6.2 Hz, 2H, Ar-H *meso*-substituent of porphyrin), 7.84–7.75 (m, 8H, Ar-H *meso*-substituent of porphyrin), 7.71 (d, *J* = 6.8 Hz, 2H, Ar-H of porphyrin), 7.54 (d, *J* = 8.3 Hz, 2H, Ar-H of porphyrin), 7.31 (t, *J* = 7.3 Hz, 2H, Ar-H of porphyrin), 7.20–6.85 (m, 20H, CHCH<sub>2</sub>CH<sub>2</sub>C<sub>6</sub>H<sub>5</sub>), 6.57 (s, 2H, Ar-H), 6.28 (s, 2H, Ar-H), 5.85 (d, *J* = 7.6 Hz, 1H, H<sub>co</sub> of OCH<sub>2</sub>O), 5.31 (d, *J* = 7.6 Hz, 2H, H<sub>bo</sub> of OCH<sub>2</sub>O), 5.11 (d, *J* = 8.3 Hz, 2H, ArOCH<sub>2</sub>Ar), 5.04 (d, *J* = 8.3 Hz, 2H, ArOCH<sub>2</sub>Ar), 4.49 (t, *J* = 8.3 Hz, 1H, CHCH<sub>2</sub>CH<sub>2</sub>C<sub>6</sub>H<sub>5</sub>), 4.32 (t, *J* = 8.3 Hz, 2H, CHCH<sub>2</sub>CH<sub>2</sub>Ph), 4.30 (s, 2H, Ar-H), 3.85 (t, *J* = 8.3 Hz, 1H, CHCH<sub>2</sub>CH<sub>2</sub>Ph), 3.18 (d, *J* = 7.6 Hz, 1H, H<sub>ci</sub> of OCH<sub>2</sub>O), 2.46 (d, *J* = 7.6 Hz, 1H, H<sub>ao</sub> of OCH<sub>2</sub>O), 2.36 (d, *J* = 9.5 Hz, 2H, H<sub>bi</sub> of OCH<sub>2</sub>O), 2.40–1.90 (m, 16H, CHCH<sub>2</sub>CH<sub>2</sub>C<sub>6</sub>H<sub>5</sub>), –0.78 (d, *J* = 7.6 Hz, 1H, H<sub>ai</sub> of OCH<sub>2</sub>O). FAB-MS: *m/z* = 1727.46 [M + H]<sup>+</sup>. Elemental analysis calcd for C<sub>110</sub>H<sub>84</sub>N<sub>4</sub>O<sub>10</sub>Pd·2H<sub>2</sub>O: C, 74.88; H, 5.03; N, 3.18%. Found: C, 75.10; H, 5.00; N, 3.35%.

**X-ray Crystallography.** The X-ray diffraction data were collected at 123 K with a Rigaku RAXIS-RAPID (1, Zntpp, and Pdcp) or RAXIS-HR (Nicip and Zncp) Imaging Plate diffractometer with graphite-monochromated Mo Kα (*λ* = 0.71075 Å) radiation. Indexing was performed from three images taken with 3° oscillation angle and exposure time 90 s per degree for 1, 60 s per degree for Zntpp and Pdcp, 15 s per degree for Nicip, and 30 s per degree for Zncp, respectively. The crystal to detector distance was 127.4 mm. Intensity data were collected by taking oscillation photographs with 4° oscillation angle for 1, 5° oscillation angle for Zntpp, Nicip, Zncp, and Pdcp, respectively. Exposure times are 600 s per degree for 1 and Pdcp, 180 s per degree for Zntpp, 60 s per degree for Nicip, and 120 s per degree for Zncp, respectively.

Structure solution and refinement were performed by “Crystal Structure” program package. Refraction data were corrected for Lorentz and polarization effects. Empirical absorption correction was applied except for Nicip. Structure was solved by direct method and refined anisotropically for non-hydrogen atoms by full-matrix least-square calculation on *F*<sup>2</sup>. The refinement was continued until all shifts were smaller than one third of the standard deviations of the parameters involved. Atomic scattering factors and anomalous dispersion terms were taken from the reference.<sup>51–53</sup> Hydrogen atoms except that of hydroxy group were located at the calculated position and were assigned a fixed displacement and constrained to ideal geometry with C–H 0.95 Å. The thermal parameters of calculated hydrogen atoms were related to those of their parent atoms by *U*(H) = 1.2*U*<sub>eq</sub>(C). 3H<sub>2</sub>O (in Zn-, Ni-, and Pdcp), a CHCl<sub>3</sub> (in Ni- and Pdcp), the encapsulated MeOH (Ni- and Pdcp), and a CH<sub>2</sub>CH<sub>2</sub>Ph (in Nicip) were disordered. The oxygen atom of MeOH that pointed metal direction in Ni- and Pdcp is discussed in this article. Methyl and phenyl protons at disordered MeOH and CH<sub>2</sub>CH<sub>2</sub>Ph were not located group, respectively. The protons of MeOH in Zntpp and Zncp were located from difference Fourier map. However, electron density corresponding protons of MeOH (in 1, Ni-, and Pdcp) and H<sub>2</sub>O (in Zn-, Ni-, and Pdcp) cannot be found by difference Fourier map. Crystallographic data and selected bond length are shown in Tables 1 and 2, respectively.

Crystallographic data have been deposited with Cambridge Crystallographic Data Centre: Deposition numbers CCDC-603776–603780. Copies of the data can be obtained free of charge via <http://www.ccdc.cam.ac.uk/conts/retrieving.html> (or from the Cambridge Crystallographic Data Centre, 12, Union Road, Cambridge, CB2 1EZ, UK; Fax: +44 1223 336033; e-mail: deposit@ccdc.cam.ac.uk).

**Determination of Guest Binding Constants, and Thermodynamic Parameters, and the Effect of Water Inhibition on Host Encapsulation.** The  $\text{CDCl}_3$  solution of **Mcp** (5 mM, 0.6 mL) and TMS was placed into a NMR tube with a gas-tight screw cap. Guest solutions or gases were introduced into the **Mcp** solution directly. The guest binding constants  $K_{11}$  was determined by  $^1\text{H}$  NMR spectra at various guest concentrations (5–50 mM) at 25 °C.<sup>11,13,54</sup> Ratios between the free and encapsulated guests were determined by the integration of their proton signals based on those of the host signals as a reference.  $[\text{Mcp}_{\text{free}}]$  were estimated from the amount of entrapped guest. The  $K_{11}$  values were calculated by the following equation.

$$K_{11} = \frac{[\text{guest}_{\text{@Mcp}}]}{[\text{Mcp}_{\text{free}}][\text{guest}_{\text{free}}]} \quad (1)$$

The average value and standard deviation of  $K_{11}$  were calculated from ten independent measurements. The results were shown in Table 4 and Fig. S9.

Since a coordinatable guest binds to **Zncp** as an axial ligand at either side of the porphyrin and tends to form the corresponding five-coordinated complex, one should take into account of the guest coordination outside of the cavity on the determination of  $K_{11}$ . Furthermore, the  $K_{11}$  values of all guests in **Zncp** were greatly affected by water concentration in the solution, because of the competitive binding of water with other guest molecules. Thus, the  $K_{11}$  for **Zncp** are calculated as the apparent value for the encapsulated guest in the cavity. Apparent binding constant of methanol in **Zncp** was observed UV–vis titration according to the literature.<sup>16,50</sup>

The degree of guest binding suppression by water was evaluated in the methane encapsulation in all **Mcp** host.  $\text{CDCl}_3$  was distilled from  $\text{CaCl}_2$  under  $\text{N}_2$  atmosphere before use.  $K_{11}$  for methane encapsulation and water concentration were measured and calculated by  $^1\text{H}$  NMR integration of guest and water signals as mentioned in  $K_{11}$  determination. The results were shown in Fig. 5.

To obtain thermodynamic parameters,  $K_{11}$  was measured as same as above method in the range between 25 and 45 °C in a 5 °C step.<sup>11,13,23</sup>  $\Delta H^\circ$  were obtained by van't Hoff plots and other parameters were calculated from  $K_{11}$  and  $\Delta H^\circ$ . The results are shown in Table 5 and Fig. S10.

This work was supported by the Grants-in-Aid for Scientific Research on Priority Areas (No. 15036254) from MEXT and for Scientific Research (A)/(S) (Nos. 14204073 and 17105003) and for Exploratory Research (No. 16655039) from JSPS as well as by a grant from The Asahi Glass Foundation. J. N. acknowledges JSPS Research Fellowship.

### Supporting Information

Crystal structure of **Zncp**, the  $\text{H}_2\text{cp}$  cavity and guests volume images,  $^1\text{H}$  NMR spectra of free **Mcps** and hydrocarbon-encapsulated ones, encapsulation of EtOH, MeCN in **Mcps**,  $K_{11}$  determination of **Zncp**– $\text{CH}_4$  system, and their van't Hoff plots. These materials are available on the web at: <http://www.csj.jp/journals/bcsj/>.

### References

- 1 M. Baik, M. Newcomb, R. A. Friesner, S. J. Lippard, *Chem. Rev.* **2003**, *103*, 2385.
- 2 R. L. Lieberman, A. C. Rosenzweig, *Nature* **2005**, *434*, 177.
- 3 T. L. Poulos, B. C. Finzel, A. J. Howard, *Biochemistry* **1986**, *25*, 5314.
- 4 J.-M. Lehn, *Supramolecular Chemistry: Concepts and Perspectives*, VCH, Weinheim, **1995**.
- 5 D. M. Rudkevich, *Angew. Chem.* **2004**, *116*, 568; *Angew. Chem., Int. Ed.* **2004**, *43*, 558.
- 6 D. J. Cram, *Nature* **1992**, *356*, 29.
- 7 P. Timmerman, W. Verboom, D. N. Reinhoudt, *Tetrahedron* **1996**, *52*, 2663.
- 8 J. Rebek, Jr., *Chem. Commun.* **2000**, 637.
- 9 J. Rebek, Jr., *Angew. Chem.* **2005**, *117*, 2104; *Angew. Chem., Int. Ed.* **2005**, *44*, 2068.
- 10 B. C. Gibb, *J. Supramol. Chem.* **2002**, *2*, 123.
- 11 N. Branda, R. Wyler, J. Rebek, Jr., *Science* **1994**, *263*, 1267.
- 12 K. Paek, C. Ihm, H. Ihm, *Tetrahedron Lett.* **1999**, *40*, 4697.
- 13 K. Paek, J. Cho, *Tetrahedron Lett.* **2001**, *42*, 1927.
- 14 A. Shivanyuk, A. Scarso, J. Rebek, Jr., *Chem. Commun.* **2003**, 1230.
- 15 A. Jasat, J. C. Sherman, *Chem. Rev.* **1999**, *99*, 931.
- 16 O. Middel, W. Verboom, D. N. Reinhoudt, *J. Org. Chem.* **2001**, *66*, 3998.
- 17 S. D. Starnes, D. M. Rudkevich, J. Rebek, Jr., *J. Am. Chem. Soc.* **2001**, *123*, 4659.
- 18 Y. Kuroda, T. Hiroshige, T. Sera, Y. Shirowa, H. Tanaka, H. Ogoshi, *J. Am. Chem. Soc.* **1989**, *111*, 1912.
- 19 J. A. A. W. Elemans, M. B. Claase, P. P. M. Aarts, A. E. Rowan, A. P. H. J. Schenning, R. J. M. Nolte, *J. Org. Chem.* **1999**, *64*, 7009.
- 20 M. C. Letzel, B. Decker, A. B. Rozhenko, W. W. Schoeller, J. Mattay, *J. Am. Chem. Soc.* **2004**, *126*, 9669.
- 21 M. Yoshizawa, M. Tamura, M. Fujita, *J. Am. Chem. Soc.* **2004**, *126*, 6846.
- 22 K. Kobayashi, K. Ishii, S. Sakamoto, T. Shirasaka, K. Yamaguchi, *J. Am. Chem. Soc.* **2003**, *125*, 10615.
- 23 R. G. Chapman, J. C. Sherman, *J. Am. Chem. Soc.* **1998**, *120*, 9818.
- 24 B. W. Purse, J. Rebek, Jr., *Proc. Natl. Acad. Sci. U.S.A.* **2005**, *102*, 10777.
- 25 M. Yoshizawa, S. Miyagi, M. Kawano, K. Ishiguro, M. Fujita, *J. Am. Chem. Soc.* **2004**, *126*, 9172.
- 26 S. Arai, H. Ohkawa, S. Ishihara, T. Shibue, S. Takeoka, H. Nishide, *Bull. Chem. Soc. Jpn.* **2005**, *78*, 2007.
- 27 J. Nakazawa, J. Hagiwara, M. Mizuki, Y. Shimazaki, F. Tani, Y. Naruta, *Angew. Chem.* **2005**, *117*, 3810; *Angew. Chem., Int. Ed.* **2005**, *44*, 3744.
- 28 L. M. Tunstad, J. A. Tucker, E. Dalcanale, J. Weiser, J. A. Bryant, J. C. Sherman, R. C. Helgeson, C. B. Knobler, D. J. Cram, *J. Org. Chem.* **1989**, *54*, 1305.
- 29 J. C. Sherman, C. B. Knobler, D. J. Cram, *J. Am. Chem. Soc.* **1991**, *113*, 2194.
- 30 P. Timmerman, H. Boerrigter, W. Verboom, G. J. VanHummel, S. Harkema, D. N. Reinhoudt, *J. Inclusion Phenom. Mol. Recognit. Chem.* **1994**, *19*, 167.
- 31 J. A. Bryant, M. Vincenti, D. J. Cram, *J. Am. Chem. Soc.* **1991**, *113*, 2167.

- 32 D. J. Cram, S. Karbach, Y. H. Kim, L. Baczynskyj, K. Marti, R. M. Sampson, G. W. Kallemeyn, *J. Am. Chem. Soc.* **1988**, *110*, 2554.
- 33 F. Tani, M. Matsu-ura, S. Nakayama, M. Ichimura, N. Nakamura, Y. Naruta, *J. Am. Chem. Soc.* **2001**, *123*, 1133.
- 34 A. D. Adler, F. R. Longo, J. D. Finarelli, J. Goldmacher, J. Assour, L. Korsakoff, *J. Org. Chem.* **1967**, *32*, 476.
- 35 E. Tsuchida, E. Hasegawa, T. Komatsu, T. Nakata, H. Nishide, *Chem. Lett.* **1990**, 389.
- 36 J. S. Lindsey, *The Porphyrin Handbook*, ed. by K. M. Kadish, K. M. Smith, R. Guilard, Academic Press, San Diego, **2000**, Vol. 1, pp. 53–55.
- 37 E. G. Azenha, A. C. Serra, M. Pineiro, M. M. Pereira, J. Seixas de Melo, L. G. Arnaut, S. J. Formosinho, A. M. d'A. R. Gonsalves, *Chem. Phys.* **2002**, *280*, 177.
- 38 A. D. Adler, F. R. Longo, F. R. Kampas, *J. Inorg. Nucl. Chem.* **1970**, *32*, 2443.
- 39 B. C. Gibb, R. G. Chapman, J. C. Sherman, *J. Org. Chem.* **1996**, *61*, 1505.
- 40 Y. Diskin-Posner, R. K. Kumar, I. Goldberg, *New J. Chem.* **1999**, *23*, 885.
- 41 M. Nishino, M. Hirota, Y. Umezawa, *The CH/π Interaction*, Wiley-VCH, New York, **1998**.
- 42 M. O. Senge, W. W. Kalisch, *Inorg. Chem.* **1997**, *36*, 6103.
- 43 A. L. Maclean, G. J. Foran, F. J. Kennedy, P. Turner, T. W. Hambley, *Aust. J. Chem.* **1996**, *49*, 1273.
- 44 E. B. Fleischer, C. K. Miller, L. E. Webb, *J. Am. Chem. Soc.* **1964**, *86*, 2342.
- 45 R. M. Silverstein, F. X. Webster, *Spectrometric Identification of Organic Compounds*, 6th ed., John Wiley & Sons, Inc., New York, **1998**.
- 46 C. J. Medforth, in *The Porphyrin Handbook*, ed. by K. M. Kadish, K. M. Smith, R. Guilard, Academic Press, San Diego, **2000**, Vol. 5, pp. 5–7.
- 47 D. J. Cram, M. E. Tanner, C. B. Knobler, *J. Am. Chem. Soc.* **1991**, *113*, 7717.
- 48 C. Ihm, M. Kim, H. Ihm, K. Paek, *J. Chem. Soc., Perkin Trans. 2* **1999**, 1569.
- 49 S. Mecozzi, J. Rebek, Jr., *Chem. Eur. J.* **1998**, *4*, 1016.
- 50 J. V. Nardo, J. H. Dawson, *Inorg. Chim. Acta* **1986**, *123*, 9.
- 51 D. T. Cromer, J. T. Waber, *International Tables for X-ray Crystallography*, The Kynoch Press, Birmingham, **1974**, Vol. IV.
- 52 J. A. Ibers, W. C. Hamilton, *Acta Crystallogr.* **1964**, *17*, 781.
- 53 D. C. Creagh, J. H. Hubbell, *International Tables for Crystallography*, Kluwer Academic Publishers, Boston, **1992**, Vol. C.
- 54 S. M. Biro, E. C. Ullrich, F. Hof, L. Trembleau, J. Rebek, Jr., *J. Am. Chem. Soc.* **2004**, *126*, 2870.